QEX

March/April 2023

www.arrl.org

A Forum for Communications Experimenters

Issue No. 337

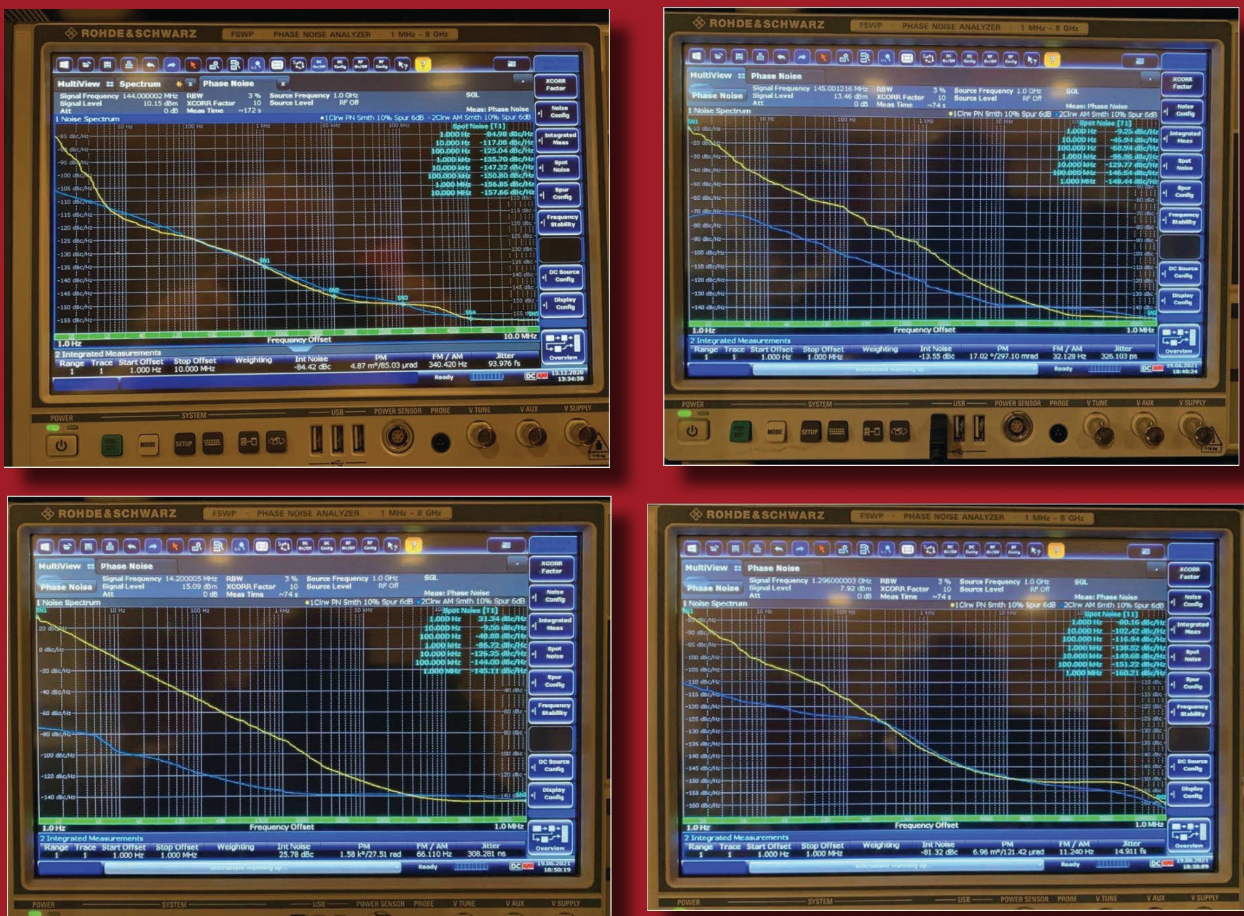

N1UL analyzes the AM and FM noise of oscillators.

KENWOOD

3rd IMDR 110 dB*

RMDR 122 dB*

BDR 150 dB*

Performance Exceeding Expectations.

The most happy and sublime encounters happen in the worst circumstances and under the harshest conditions.

There are enthusiasts who know this all too well because of their love of HF radio.

Results born of certainty and not circumstance. Delivered through impeccable performance. This is our offering to you.

"The Kenwood TS-890S has the highest RMDR of any radio I have ever measured."
- Rob Sherwood - NC0B - December 2018

HF/50MHz TRANSCEIVER
TS-890S

Top-class receiving performance

3 kinds of dynamic range make for top-class performance.

- Third order intermodulation Dynamic Range (3rd IMDR) 110dB*
- Reciprocal Mixing Dynamic Range (RMDR) 122dB*
- Blocking Dynamic Range (BDR) 150dB*

*Values are measured examples. (2kHz spacing:14.1 MHz, CW, BW 500 Hz, Pre Amp OFF)

- Full Down Conversion RX
- High Carrier to Noise Ratio 1st LO
- H-mode mixer

4 kinds of built-in roofing filters

500Hz / 2.7kHz / 6kHz / 15kHz (270Hz Option)

7 inch Color TFT Display

- Roofing frequency sampling band scope
- Band scope auto-scroll mode
- Multi-information display including filter scope

Clean and tough 100W output

Built-in high-speed automatic antenna tuner

32-bit floating-point DSP for RX / TX and Bandscope

*: 2 kHz spacing measurement standard - Receiver frequency 14.2 MHz, MODE CW, BW 500 Hz, PRE AMP OFF

Customer Support: (310) 639-4200

www.kenwood.com/usa

JQA-1205 091 ISO9001 Registered JVCKENWOOD Corporation

ADS#16221

QEX

March/April 2023

QEX (ISSN: 0886-8093) is published bimonthly in January, March, May, July, September, and November by the American Radio Relay League, 225 Main St., Newington, CT 06111-1400. Periodicals postage paid at Hartford, CT and at additional mailing offices.

POSTMASTER: Send address changes to: QEX, 225 Main St., Newington, CT 06111-1400
Issue No. 335

Publisher
American Radio Relay League

Kazimierz "Kai" Siwiak, KE4PT
Editor

Lori Weinberg, KB1EIB
Assistant Editor

Ray Mack, W5IFS
Contributing Editors

Production Department

Becky R. Schoenfeld, W1BXY
Director of Publications and Editorial

Michelle Bloom, WB1ENT
Production Supervisor

David Pingree, N1NAS
Senior Technical Illustrator

Brian Washing
Technical Illustrator

Advertising Information

Janet L. Rocco, W1JLR
Business Services
860-594-0203 – Direct
800-243-7768 – ARRL
860-594-4285 – Fax

Circulation Department

Cathy Stepina
QEX Circulation

Offices

225 Main St., Newington, CT 06111-1400 USA
Telephone: 860-594-0200
Fax: 860-594-0259 (24-hour direct line)
Email: **qex@arrl.org**

Subscription rate for 6 print issues:

In the US: $29

US by First Class Mail: $40;

International and Canada by Airmail: $35

ARRL members receive the digital edition of *QEX* as a member benefit.

In order to ensure prompt delivery, we ask that you periodically check the address information on your mailing label. If you find any inaccuracies, please contact the Circulation Department immediately. Thank you for your assistance.

About the Cover

Dr. Ulrich L. Rohde, N1UL, emphasizes the importance of knowing what type of noise to look for when using signal generators for measurements. N1UL uses Harmonica Simulator (Ansoft) to predict both the AM and FM phase noise of oscillators. He duplicates the details of the actual circuit in the simulator model, and at 144 MHz looks at the three critical offset values: 1 kHz, 10 kHz and 100 kHz. N1UL shows the measured AM and FM phase noise of LC VHF, and 14 MHz oscillators. Measure-ments additionally show the currently best possible performance of a 1296 MHz oscillator.

In This Issue

Index of Advertisers

The American Radio Relay League

The American Radio Relay League, Inc., is a noncommercial association of radio amateurs, organized for the promotion of interest in Amateur Radio communication and experimentation, for the establishment of networks to provide communications in the event of disasters or other emergencies, for the advancement of the radio art and of the public welfare, for the representation of the radio amateur in legislative matters, and for the maintenance of fraternalism and a high standard of conduct.

ARRL is an incorporated association without capital stock chartered under the laws of the state of Connecticut, and is an exempt organization under Section 501(c)(3) of the Internal Revenue Code of 1986. Its affairs are governed by a Board of Directors, whose voting members are elected every three years by the general membership. The officers are elected or appointed by the Directors. The League is noncommercial, and no one who could gain financially from the shaping of its affairs is eligible for membership on its Board.

"Of, by, and for the radio amateur," ARRL numbers within its ranks the vast majority of active amateurs in the nation and has a proud history of achievement as the standard-bearer in amateur affairs.

A *bona fide* interest in Amateur Radio is the only essential qualification of membership; an Amateur Radio license is not a prerequisite, although full voting membership is granted only to licensed amateurs in the US.

Membership inquiries and general correspondence should be addressed to the administrative headquarters:

ARRL
225 Main St.
Newington, CT 06111 USA
Telephone: 860-594-0200
FAX: 860-594-0259 (24-hour direct line)

Officers

President: Rick Roderick, K5UR
P.O. Box 1463, Little Rock, AR 72203

The purpose of *QEX* is to:

1) provide a medium for the exchange of ideas and information among Amateur Radio experimenters,

2) document advanced technical work in the Amateur Radio field, and

3) support efforts to advance the state of the Amateur Radio art.

All correspondence concerning *QEX* should be addressed to the American Radio Relay League, 225 Main St., Newington, CT 06111 USA. Envelopes containing manuscripts and letters for publication in *QEX* should be marked Editor, *QEX*.

Both theoretical and practical technical articles are welcomed. Manuscripts should be submitted in word-processor format, if possible. We can redraw any figures as long as their content is clear. Photos should be glossy, color or black-and-white prints of at least the size they are to appear in *QEX* or high-resolution digital images (300 dots per inch or higher at the printed size). Further information for authors can be found on the Web at **www.arrl.org/qex/** or by e-mail to **qex@arrl.org**.

Any opinions expressed in *QEX* are those of the authors, not necessarily those of the Editor or the League. While we strive to ensure all material is technically correct, authors are expected to defend their own assertions. Products mentioned are included for your information only; no endorsement is implied. Readers are cautioned to verify the availability of products before sending money to vendors.

Kazimierz "Kai" Siwiak, KE4PT

Perspectives

Communicate with the Author

Author Alan Victor, W4AMV, writes to us:

"I just came across by accident the **groups.io** that addresses *QEX* papers. I was happy to see so much discussion and confusion on my paper, "A Systematic Design Approach to RF Power Amplifiers," from July/August 2021 *QEX*. It is clear that the key takeaway concepts were missed and I understand and appreciate the commentary. The problem I have is quite simple. My email address is located in the masthead. If there are questions or concerns or clarifications required, then by all means contact the author! The (**groups.io**) moderator ... never attempted to contact me. That's too bad! ..."

Alan continues:

"My suggestion for an editorial is ... if there are questions about a topic, or you the reader need clarification, by all means contact the author. Contact information is always provided. Seems a shame this even needs mentioning!"

The *QEX* editor agrees with Alan. Please make every effort to include the author in your discussions, questions and comments. After all, *QEX* is "A Forum for Communications Experimenters." The digital edition of *QEX* is available on-line free of charge for all ARRL members, and the printed edition is available to subscribers.

In This Issue:

- H. Lawrence Serra, N6NC, correlates take-off angles and received angles of arrival with a make-do interferometer.
- Dr. Ulrich L. Rohde, N1UL, analyzes and measures AM and FM noise of oscillators.
- Wesley Cardone, N8QM, Characterizes the generic diode with precision for simulation using SPICE.
- Jeff Anderson, K6JCA, Corrects a common L-network misconception.
- Glen Schulz, W9IQ, in a Technical Note discusses the Smith Chart SWR circle.
- Ron Block, NR2B, discusses the single point ground panel location.
- Eric P. Nichols, KL7AJ, in his Essay Series discusses phase.
- Wojciech Kaczmarski, SP5WWP, and James T. Francis, Jr., KA1PQK, Nyquist filter.

Writing for QEX

Please continue to send in full-length *QEX* articles, or share a **Technical Note** of several hundred words in length plus a figure or two. *QEX* is edited by Kazimierz "Kai" Siwiak, KE4PT, (**ksiwiak@arrl.org**) and is published bimonthly. *QEX* is a forum for the free exchange of ideas among communications experimenters. All members can access digital editions of all four ARRL magazines: *QST*, *OTA, QEX*, and *NCJ* as a member benefit. The *QEX printed edition* is available at an annual subscription rate (6 issues per year) for members and non-members, see **www.arrl.org/qex**.

Would you like to write for *QEX*? We pay $50 per published page for full articles and *QEX* Technical Notes. Get more information and an Author Guide at **www.arrl.org/qex-author-guide**. If you prefer postal mail, send a business-size self-addressed, stamped (US postage) envelope to: *QEX* Author Guide, c/o Maty Weinberg, ARRL, 225 Main St., Newington, CT 06111.

Very kindest regards,

Kazimierz "Kai" Siwiak, KE4PT

QEX Editor

Dr. Ulrich L. Rohde, N1UL
990 Cape Marco Dr., PH2, Marco Island, FL 34145; **Dr.Ulrich.L.Rohde@gmail.com**

AM and FM Noise in Oscillators

It is important to know what type of noise to look for when using signal generators for measurements.

When measuring the single side band (SSB) noise of oscillators, until recently all specifications were in reference to FM noise at specific offsets of the carrier in modern signal generators. Vector signal generators have a base band in which the various types of modulations are created, and then added/mixed to the wanted output frequency. Such modern signal generators are available to 74 GHz and higher. They are frequently used to determine the dynamic range of a receiver, specifically the blocking dynamic range.

Blocking is defined as the degradation of receiver sensitivity, usually by 3 dB, in the presence of a much stronger (blocking) signal. Therefore we must first understand that sensitivity is the measure of the smallest possible detectable signal. Sensitivity is measured through signal-to-noise ratio (SNR) at the output of the receiver. Different SNR values can be chosen according to the specific task. Blocking would therefore be the reduction in SNR caused by an interfering signal **[1]**.

ACPR

Another more modern test method is the determination of the "Adjacent Carrier Power Ratio" (ACPR). It is the ratio between the total power in adjacent channels (intermodulation signal) to the main channel's power (wanted signal). There are two ways of measuring ACPR. The first way is by finding 10×log of the ratio of the total output power to the power in adjacent channel. The second (and much more popular method) is to find the ratio of the output power in a smaller bandwidth around the carrier center, to the power in the adjacent channel. The smaller bandwidth is equal to the bandwidth of the adjacent channel signal. The second way is more popular, because it can be measured easily. ACPR is desired to be as low as possible. A high ACPR indicates that significant spectral spreading has occurred.

When evaluating receivers by measuring their oscillator's noise there is a distinct difference between AM and FM noise generated in the generator used for the ACPR eluting. Now being alerted about how to the design a good low AM noise generator, let us consider the following. The resulting oscillator will be best using tunable *LC* (helical resonator) based oscillators (VCOs) and field effect transistors. In this paper we want to show a mathematical approach to derive this information, and will rely on Chapter 8 of a dissertation **[2]**. We will retain the figure and equation numbering in **[2]**.

Phase Noise Analysis Based on the Negative Noisy Resistance Model

We now refer to Chapter 8 of "A New and Efficient Method of Designing Low Noise Microwave Oscillators," **[2]**. The following noise analysis for the oscillator, while based on the approach of Kurokawa **[3]**, is an attempt to introduce the concept of a "noisy" negative resistance that is time dependent. This was first proposed by Kurokawa, addressing the question of synchronized oscillators, provided insight in the general case of a series oscillator. The method introduced here is specific for a real oscillator and real noise sources.

This concept gets started by connecting a parallel-tuned circuit to a transistor in Colpitts configuration, Figure 8-2 in **[2].** Since, the two capacitors C1 and C2 are similar in value, not different by more than a factor of 2 or 3, and connected to a parallel-tuned circuit via a small coupling capacitor Cc, the output impedance of the emitter follower circuit gets transformed to the base. The differential output impedance at the emitter is $1/Y_{21}{}^{+}$ (large signal), while the input impedance itself is $\beta/Y_{21}{}^{+}$. Because of this, the contribution of Y_{21} can be neglected for the basic analysis. This is valid only for this particular case. Consistent with Equation (6-1) in **[2]**, which is based on the same approximation, but includes the parasitics, the transistor circuit now provides negative resistance (or a negative conductance). This negative conductance cancels the losses concentrated in the loss resistor R_P, which for infinite Q would also be infinite.

Figure 8-2 in **[2]** is a Colpitts oscillator arrangement, simplified for the purpose of showing the circuit components. On the left side we see the resonator tank circuit with the loss resistor R_P, and on the right side we see the negative conductance, which is time dependent. The time dependence comes from the fact that the collector current is a series of pulses and the negative conductance is only present during a small period of time. This explanation is necessary to justify the existence of a loaded Q. If there would be a negative resistance or conductance present all the time, the compensating circuit would reduce the bandwidth to essentially zero or an infinite Q. In reality, however, for most of the time the transistor "loads" the tuned circuit, and therefore, the operating Q is less than the unloaded Q.

The two circuits of Figure 8-3 in **[2]**

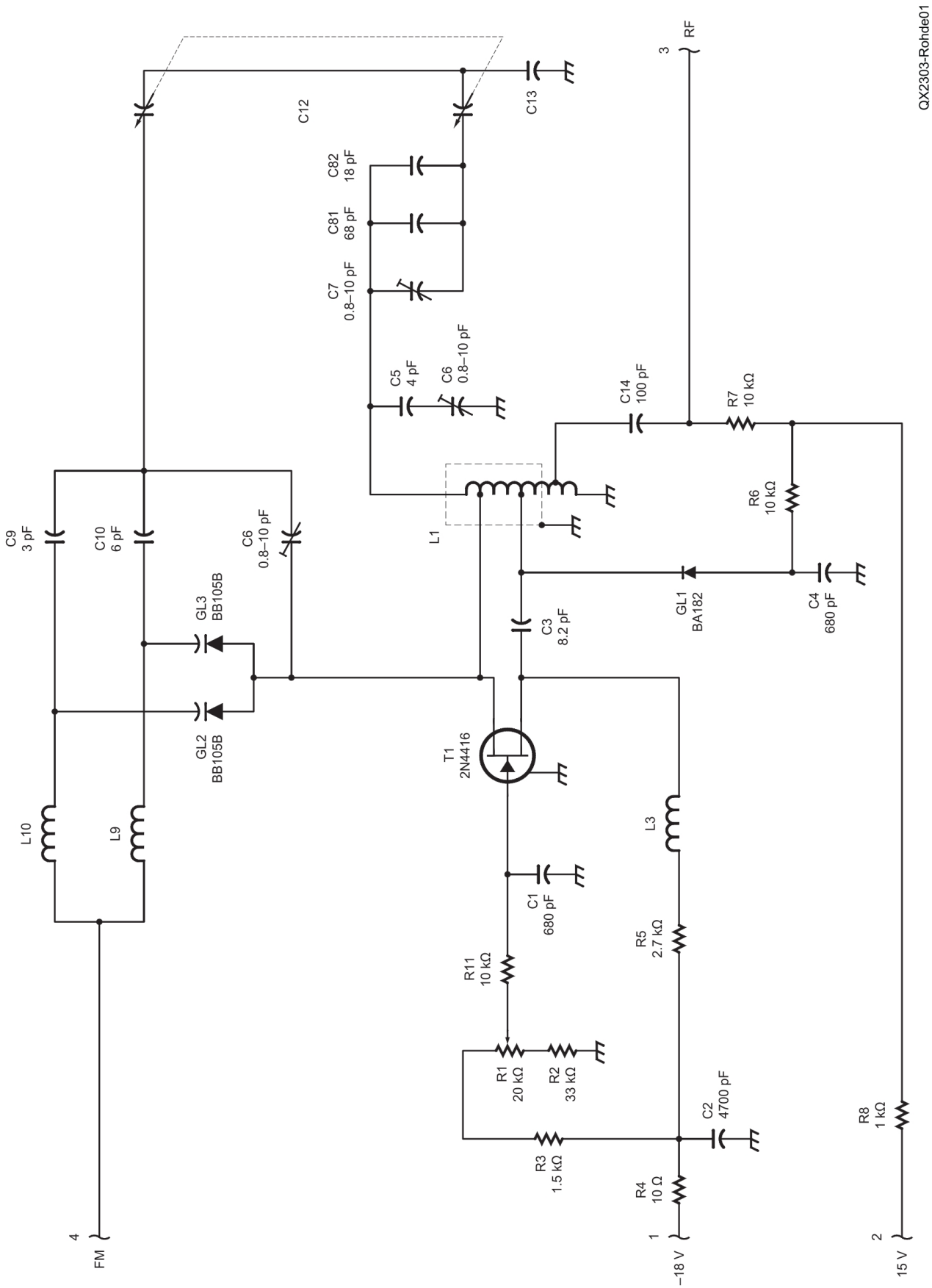

Figure 1 – Typical high performance 144 MHz oscillator circuit.

show the transition from a series tuned circuit connected with the series time-dependent negative resistance as outlined in Equation (6-1) in **[2]**, and the resulting input capacitance labeled C_{IN}. Translated, the resulting configuration consists of a series circuit with inductance L and the resulting capacitance C'. The noise voltage $e_N(t)$ describes a small perturbation, which is the noise resulting from R_L and $-R_N(t)$.

Figure 8-3 in **[2]** shows the equivalent representation of the oscillator circuit in the presence of noise. The circuit equation of the oscillator circuit of Figure 8-3 in **[2]** can be given as

$$L\frac{di(t)}{dt}+\left(R_L-R_N(t)\right)i(t)+\frac{1}{C}\int(t)dt=e_N(t) \tag{8-11}$$

where $i(t)$ is the time varying resultant current. Due to the noise voltage $e_N(t)$, Eq. 8-11 is a non-homogeneous differential equation. If the noise voltage is zero, it translates into a homogeneous differential equation.

The rather extensive analytical development of phase noise continues throughout Chapter 8 of **[2]**. I transition now to a practical example.

A Practical Example

To predict the phase noise of the oscillator shown in **Figure 1**, I have used the Harmonica Simulator (*Ansoft*) and duplicated the details of the actual circuit in the model seen in **Figure 2**. At 144 MHz we look at the three critical offset values: 1 kHz, 10 kHz and 100 kHz. **Figure 3** shows simulation results for the phase noises –120 dBc/Hz, –140 dBc/Hz and –160 dBc/Hz respectively. **Figure 4** shows simulated output power.

Figure 5 shows measured phase noise of an *LC* VHF oscillator. Because of the influence of the tuning diodes the measured noise differs from the prediction. The yellow (upper curve at low frequencies) line is the FM noise, the blue (lower) is the AM noise. The AM noise is caused by the ALC circuit and does not affect the performance significantly.

Figure 6 shows a 14 MHz *LC* oscillator measurement. The noise contribution of a digitally generated signal has a huge value. Here the yellow (lower) curve is the phase noise that is typically shown in the datasheet, but the high AM noise (upper curve) is not mentioned. If using this generator to measure the ACPR one would get a poor value for a probably much better

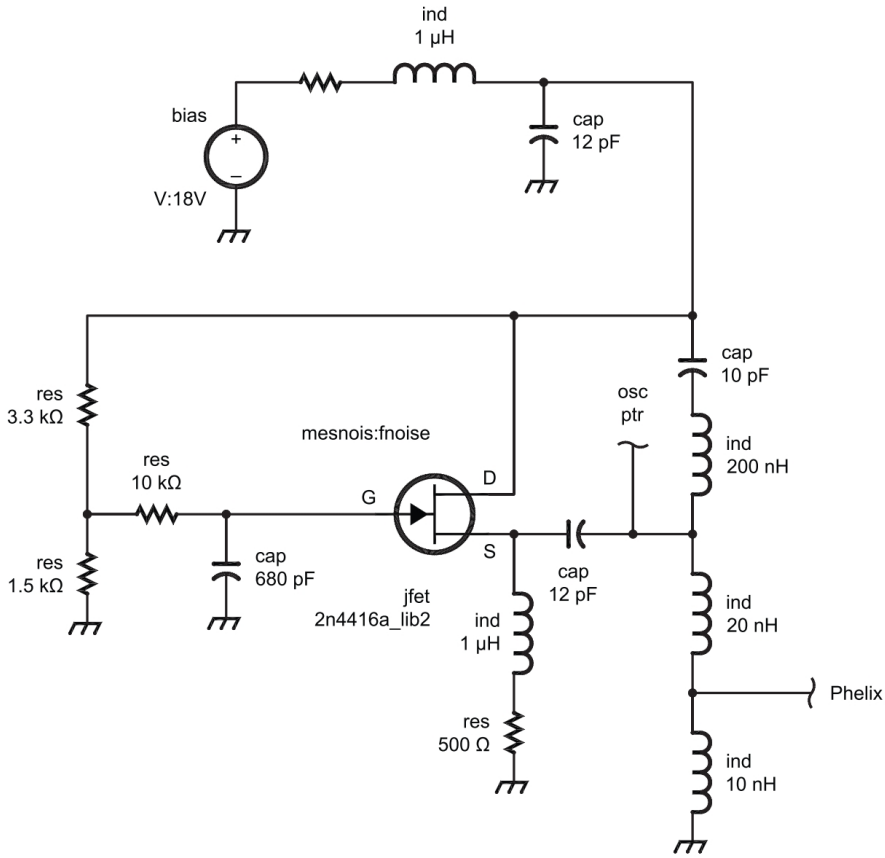

Figure 2 – Oscillator of Figure 1 prepared for the simulator.

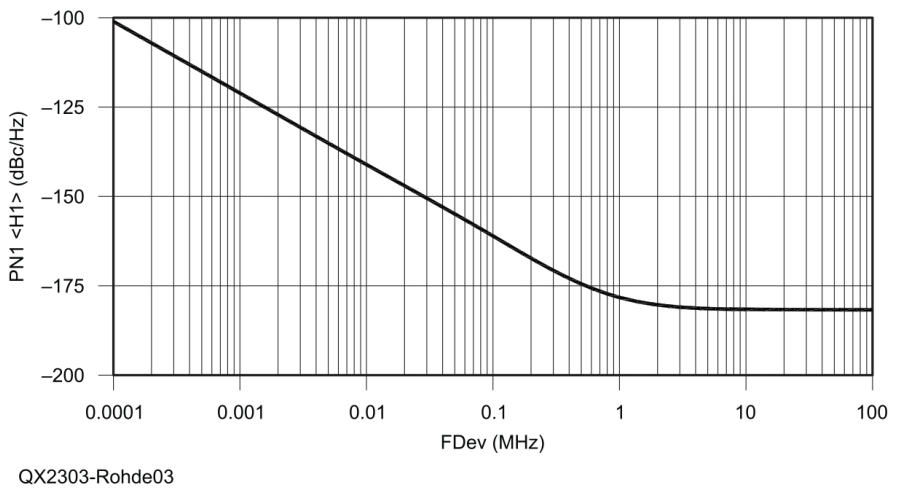

Figure 3 – Phase noise simulation result for the circuit of Figure 2. Specifically, at 1, 10, and 100 kHz the phase noises are –120 dBc/Hz, –140 dBc/Hz and –160 dBc/Hz respectively.

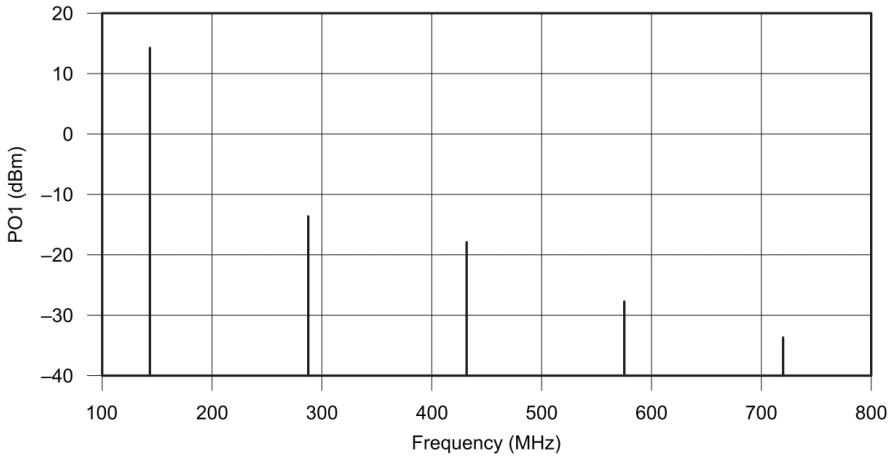

Figure 4 – Output power simulation.

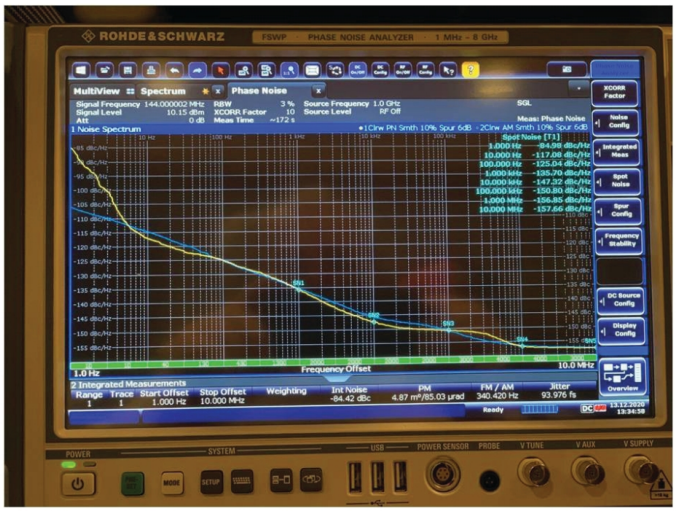

Figure 5 – Measured phase noise of an *LC* VHF oscillator. The yellow (upper curve at low frequencies) line is the FM noise, the blue (lower) is the AM noise.

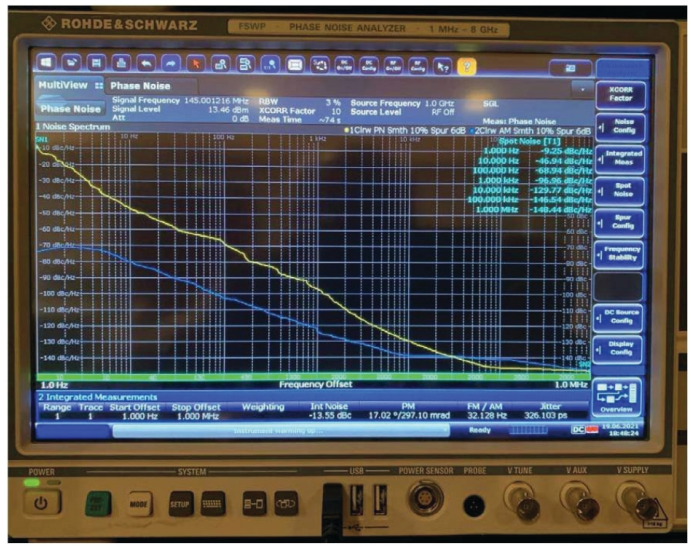

Figure 7 – VHF FM (yellow upper curve) and AM (blue lower curve) noise plots for the circuit of Figure 2.

Figure 6 – 14 MHz FM and AM noise plot of a modern digital signal processing based signal generator. Here the yellow line again is the phase noise, that is typically shown in the datasheet, but the high AM (blue upper curve) noise is not mentioned.

Figure 8 – The currently best possible performance of a 1296 MHz oscillator. This is not a generator using IQ modulators.

device under test.

Figure 7 shows VHF FM (upper curve) and AM (lower curve) noise plots. **Figure 8** shows the currently best possible performance of a 1296 MHz oscillator. This is not a generator using IQ modulators.

For further reading please see Prof. Ali M. Niknejad, "Oscillator Phase Noise" **[4]**.

Prof. Dr. Ing. habil Ulrich L. Rohde, N1UL, is a partner of Rohde & Schwarz, Munich Germany, Chairman of Synergy Microwave Corp., Paterson, New Jersey, President of Communications Consulting Corporation, serving as an honorary member of the Senate of the University of the Armed Forces Munich, Germany honorary member of the Senate of the Brandenburg University of Technology Cottbus–Senftenberg, Germany, past member of the Board of Directors of Ansoft Corporation, Pittsburgh, Pennsylvania.

Dr. Rohde is serving as a Professor of Radio-Microwave Frequency Theory and Techniques at several universities worldwide, to name a few: Honorary Professor IIT-Delhi, Honorary Chair Professor IIT-Jammu, Professor at the University or Oradea for microwave technology, an honorary professor at the BTU Cottbus-Senftenberg University of Technology, and professor at the German Armed Forces University Munich (Technical Informatics).

Dr. Rohde has published 300+ scientific papers, co-authored over dozen books, and has produced dozens of patents, received several awards, including: recipient of 2019 IETE Fellow Award, 2019 IEEE CAS Industrial Pioneer Award, 2017 RCA Life time achievement award, 2017 IEEE-Cady Award, 2017 IEEE AP-S Distinguish achievement award, 2016 IEEE MTT-S Applications Award, 2015 IEEE-Rabi Award, 2015 IEEE Region-1 Award, and 2014 IEEE-Sawyer Award.

In 2006, Dr. Rohde was honored as Microwave Legend by Microwave & RF Magazine, the selection was based on global voting. In 2009, Dr. Rohde was selected in the list of Divine Innovators of November 2011, Microwave Journal. Based on Dr. Rohde's 5-decade of scientific creativity and pioneer contributions in the field of microwave communications systems and antenna, IEEE has established 3 awards in his name — the IEEE Ulrich L. Rohde Innovative Conference Paper Awards on Antenna Measurements and Applications and the IEEE Ulrich L. Rohde Innovative Conference Paper Awards on Computational Techniques in Electromagnetics, and IEEE Ulrich L. Rohde Humanitarian Technical Field Project Award. His hobbies are sailing, U.S. Merchant Marine Officer, Master of Steam or Motor Vessels, photography and amateur radio.

References

[1] **https://www.microwaves101.com/encyclopedias/receiver-blocking**.

[2] Ulrich L. Rohde, "A New and Efficient Method of Designing Low Noise Microwave Oscillators", Upper Saddle River, NJ USA, **https://depositonce.tu- berlin.de/bitstream/11303/1306/1/Dokument_16.pdf**.

[3] K. Kurokawa, "Some Basic Characteristics of Broadband Negative Resistance Oscillator Circuits," Bell Syst. Tech. Journal, pp. 1937- 1955, July-August 1969.

[4] **rfic.eecs.berkeley.edu/~niknejad/ee242/pdf/eecs242_lect22_phasenoise.pdf**.

Jeff Anderson, K6JCA

1215 Carmel Terrace, Los Altos, CA 94024; **jca1955@sbcglobal.net**

Correcting a Common L-Network Misconception

Guidelines are corrected, that are commonly used to determine if a Series-Parallel or a Parallel-Series configuration should be chosen.

This article examines the commonly-used criteria for selecting an L-Network configuration (Series-Parallel versus Parallel-Series) and will point out that these guidelines are actually incorrect. Equations will then be derived for calculating the elements of either L-Network configuration, and in the process of these derivations the incorrect selection criteria will be corrected.

In addition, an alternative derivation of the equations for a Series-Parallel network will be presented that results in equations that are more in line with those derived for the Parallel-Series network.

Finally, an example will be presented in which an impedance is transformed using both Series-Parallel and Parallel-Series L-Network equations.

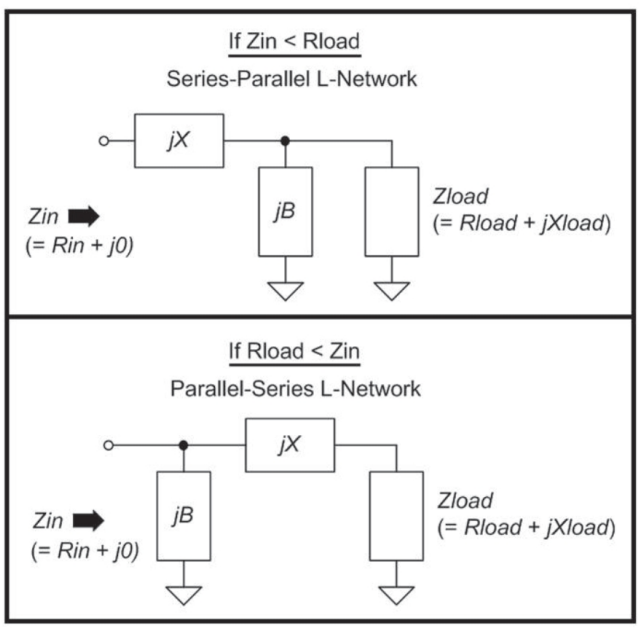

Figure 1 — Original criteria for selecting an L-Network configuration.

The Original Criteria for Selecting an L-Network Configuration

L-Networks provide a basic way to transform one impedance to another. This discussion will assume that the impedance to be transformed, *Zload*, is a complex value (i.e. *Zload* = *Rload* + *j Xload*) whose real component, *Rload*, is never negative, and that *Zin*, the impedance to which *Zload* is to be transformed — (as measured at the L-Network's input port), is a real value, with no reactive component, i.e. *Zin* = *Rin* + *j* 0.

L-Networks can be configured in two ways, as a Series-Parallel network or as a Parallel-Series network. Referring to **Figure 1**, the common criteria **[1]**, **[2]**, **[3]** for selecting which network configuration to use, given a specific load impedance, are:

1) Use a Series-Parallel L-Network when *Rin* < *Rload*.

2) Use a Parallel-Series L-Network when *Rload* < *Rin*.

For example, given these criteria, if *Zload* is to be transformed to Z_0 (a real, not complex, value, e.g. 50 + *j* 0 Ω), then *Zin* = Z_0 and a Series-Parallel L-Network should be used when Z_0 < *Rload*. Otherwise, use a Parallel-Series network when *Rload* < Z_0.

The impedances that satisfy these two criteria can be plotted on Smith Charts, see **Figure 2**. Note that these impedances, when

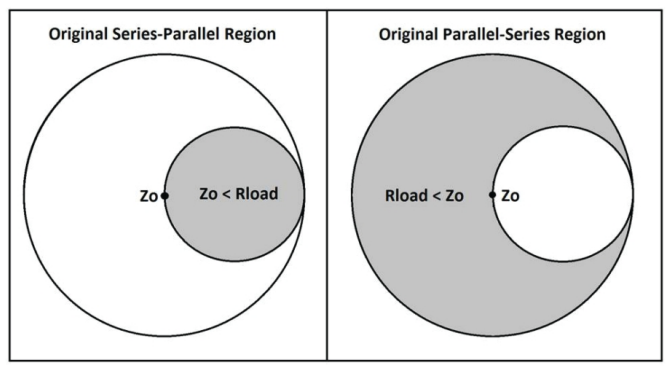

Figure 2 — Smith Chart Impedance Regions (in grey) for the original L-Network selection criteria. The two regions are mutually exclusive.

combined, span the entire Smith Chart — except for any load impedance whose *Rload* equals Z_0 — and that they are separated into two mutually exclusive regions.

The Correct Criteria for Selecting an L-Network Configuration

But these commonly used criteria are not correct. For example, when transforming *Zload* to Z_0, the guideline should not be to use a Series-Parallel L-Network when $Z_0 < Rload$. Instead, a Series-Parallel network should be chosen when

$$\frac{Rload}{Rload^2 + Xload^2} \leq \frac{1}{Z_0}$$

Or, stated more succinctly, when

$$Gload \leq \frac{1}{Z}$$

original Parallel-Series selection criteria: $Rload < Z_0$.

As shown in **Figure 3**, the correct criteria for selecting a Parallel-Series or Series-Parallel L-Network (when matching *Zload* to Z_0) should be:

1) Select Series-Parallel when $Gload \leq 1/Z_0$.

2) Select Parallel-Series when $Rload \leq Z_0$.

Note that the "≤" inequality comes directly from the L-Network equations (derived below), and its use results in matching solutions — be they two-component or reduced to a single component — for all impedances within the Smith Chart.

The impedances associated with these new criteria, plotted on Smith Charts, are shown in **Figure 4**. Note that these regions agree with the impedance regions described by H. Ward Silver, NØAX, in his "Hands-On Radio" column in the February 2008 issue of *QST* **[4]**.

One result of the new criteria is that impedances that satisfy each of these two criteria are no longer separated into two mutually-exclusive regions on the Smith Chart. Now there is a significant

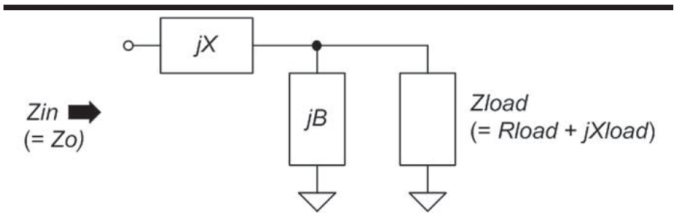

Figure 6 — The Series-Parallel L-Network used for deriving the equations.

assume this network is to transform *Zload* to be Z_0, a real, not complex, value, i.e. let *Zin* = Z_0, e.g. 50 + *j* 0 Ω. Making this substitution and also recognizing that *Zload* = *Rload* + *jXload*, **Eqn (1)** becomes:

$$Z_0 = jX + \frac{1}{jB + \frac{1}{Rload + jXload}} \qquad (2)$$

Expand **Eqn (2)**. Then, from this new equation collect the real terms on either side of the equals sign, which will result in the following equation:

$$B\left(X \bullet Rload - Xload \bullet Z_0\right) = Rload - Z_0 \qquad (3)$$

The collected imaginary terms on either side of the same expanded equation are rearranged to solve for *X*:

$$X = \frac{B \bullet Z_0 \bullet Rload - Xload}{1 - B \bullet Xload} \qquad (4)$$

Eqn (4) can then be substituted into **Eqn (3)**. The resulting equation, when expressed in terms of *B*, will be of the form:

$$aB^2 + bB + c = 0$$

The solution for *B* in this equation has two roots:

$$B = \frac{Xload \pm \sqrt{\frac{Rload}{Z_0}}\sqrt{Rload^2 + Xload^2 - Z_0 \bullet Rload}}{Rload^2 + Xload^2} \qquad (5)$$

B must be a real number. That is, since *jB* is imaginary, *B* without the *j* multiplier must be real. If *B* is to be real, the quantity under the second square root sign cannot be negative. It must satisfy the condition:

$$Rload^2 + Xload^2 - Z_0 \bullet Rload \geq 0 \qquad (6)$$

At this point references (e.g. **[7]**, **[8]**, **[9]**) typically state that *Rload* > Z_0 satisfies **Eqn (6)**. Thus a Series-Parallel L-Network should be selected when *Rload* > Z_0, and indeed, *Rload* > Z_0 does satisfy **Eqn (6)**. But *Rload* > Z_0 is really just a subset of the full set of load-impedances that satisfy **Eqn (6)**.

To find this full set of impedances, simply rearrange **Eqn (6)** to become:

$$\frac{Rload}{Rload^2 + Xload^2} \leq \frac{1}{Z_0} \qquad (7)$$

If a load-impedance meets this new criteria, it can then be transformed with a Series-Parallel L-Network, even if it fails the original *Rload* > Z_0 criteria.

We can reduce **Eqn (7)** to an even simpler form. First, recognize that the quantity

$$\frac{Rload}{Rload^2 + Xload^2}$$

is equivalent to the conductance value *Gload* if the load-impedance, *Zload*, were converted to an equivalent load-admittance, *Yload*. That is,

$$Yload = Gload + jBload = \frac{1}{Zload} = \frac{Rload}{Rload^2 + Xload^2} - \frac{jXload}{Rload^2 + Xload^2}$$

Substituting *Gload* into **Eqn (7)** for the quantity on the left side of the "≤" symbol, we arrive at the final form of the criteria for selecting a Series-Parallel L-Network:

$$Gload \leq \frac{1}{Z_0} \qquad (8)$$

Deriving the Parallel-Series L-Network Equations

Equations for a Parallel-Series L-Network can be similarly derived (again, the series and parallel components are assumed to be lossless) using equations derived from **Figure 7**.

Referring to **Figure 7**, *Zin* is the impedance (real, not complex) looking into the network's input:

$$Zin = \frac{1}{jB + \frac{1}{Rload + j\left(Xload + X\right)}} \qquad (9)$$

If we are transforming *Zload* to Z_0 (e.g. 50 + *j* 0 Ω), then this equation becomes:

$$Z_0 = \frac{1}{jB + \frac{1}{Rload + j\left(Xload + X\right)}} \qquad (10)$$

We can expand this equation to be:

$$Z_0 + jB \bullet Z_0 \bullet Rload - B \bullet Z_0 \bullet \left(Xload + X\right) = Rload + j\left(Xload + X\right) \qquad (11)$$

The next step is to separate out the real and imaginary terms on both sides of **Eqn (11)**. The collected real terms on either side of the equation are:

$$Z_0 - B \bullet Z_0 \bullet \left(Xload + X\right) = Rload \qquad (12)$$

The collected imaginary terms on either side of the equation are rearranged to solve for *X*:

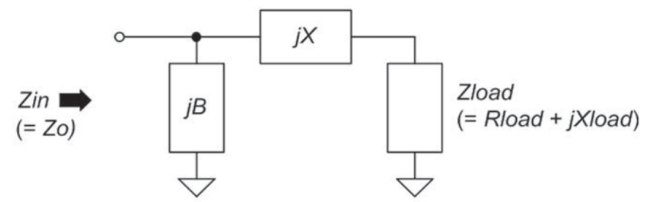

Figure 7 — The Parallel-Series L-Network used for deriving the equations.

$$X = B \bullet Z_0 \bullet Rload - Xload \qquad (13)$$

We can substitute **Eqn (13)** into **Eqn (12)** and rearrange in terms of *B*. The result will be an equation of the form $aB^2 + c = 0$. Its two roots are:

$$B = \frac{\pm\sqrt{\frac{Z_0 - Rload}{Rload}}}{Z_0} \qquad (14)$$

Again, *B* must be a real number. For this condition to be satisfied, the quantity under the square root must not be negative, which means that the following equation must be true:

$$Z_0 - Rload \geq 0 \qquad (15)$$

which becomes,

$$Rload \leq Z_0 \qquad (16)$$

Note that this new criteria is almost identical to the original Parallel-Series L-Network selection criteria, stated at the start of this article (with the exception that the original "<" symbol is now "≤").

An Alternative Derivation of the Equations for a Series-Parallel L-Network

Given the apparent duality of the Smith Chart regions for the impedances associated with the new criteria — one region is the mirror image of the other, see **Figure 4** — I wondered if there might be a better way to derive the Series-Parallel L-Network equations that did not result in awkward equations such as **Eqn (5)**.

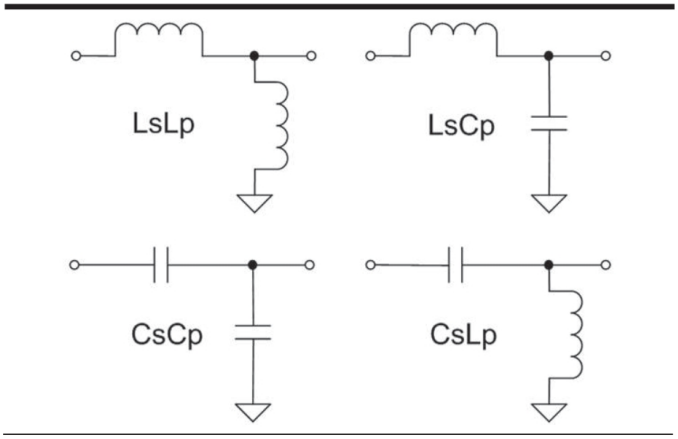

Figure 8 — The four Series-Parallel L-Networks.

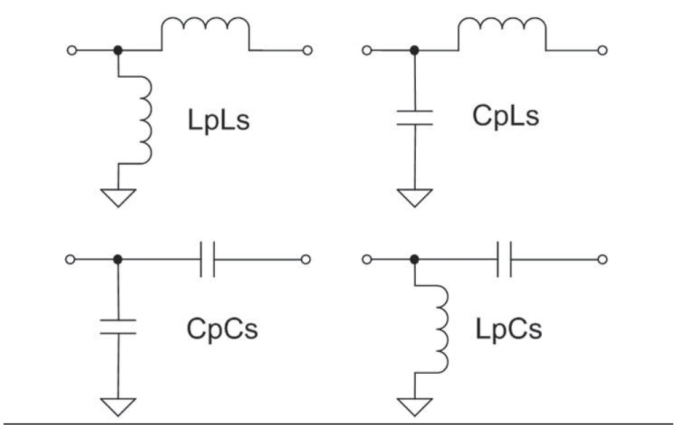

Figure 9 — The four Parallel-Series L-Networks.

Let us again draw a Series-Parallel L-Network, but this time express the load and input impedances as admittances, as shown in **Figure 10**. The equation for *Yin* is:

$$Yin = \frac{1}{jX + \frac{1}{Gload + j\left(Bload + B\right)}} \qquad (17)$$

If transforming *Zload* to Z_0, this equation becomes:

$$\frac{1}{Z_0} = \frac{1}{jX + \frac{1}{Gload + j\left(Bload + B\right)}} \qquad (18)$$

Expand **Eqn (18)**. Then, from this new equation collect the real terms on either side of the equals sign, which will result in the following equation:

$$\frac{1}{Z_0} - Gload = \left(\frac{1}{Z_0}\right) X \left(Bload + B\right) \qquad (19)$$

Similarly, collecting the imaginary terms on either side of the same equation results in the following equation, rearranged to solve for *B*:

$$B = \left(\frac{1}{Z_0} \bullet X \bullet Gload\right) - Bload \qquad (20)$$

Insert **Eqn (20)** into **Eqn (19)** and then rearrange in terms of *X*. The result is an equation of the form $aX^2 + c = 0$ that has two roots:

$$X = \pm Z_0 \sqrt{\frac{\frac{1}{Z_0} - Gload}{Gload}} \qquad (21)$$

Note that for *X* to be real, the quantity under the square root must not be negative. That is, the following equation must be true:

$$\frac{1}{Z_0} - Gload \geq 0 \qquad (22)$$

Rearranging this equation, we have the criteria for selecting a Series-Parallel L-Network:

$$Gload \leq \frac{1}{Z_0} \qquad (23)$$

Note the similarities between the new Series-Parallel **Eqns (20)**, **(21)**, and **(23)** and the Parallel-Series **Eqns (13)**, **(14)**, and **(16)**. There is clearly a duality between the two network configurations

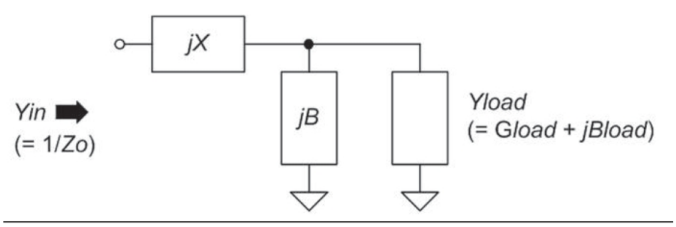

Figure 10 — Alternative Series-Parallel circuit for Series-Parallel equation derivation using input-admittance (*Yin*) and load-admittance (*Yload*).

that wasn't obvious when comparing the original Series-Parallel **Eqns (4)**, **(5)**, and **(7)** with the Parallel-Series **Eqns (13)**, **(14)**, and **(16)**. See **Table 1**.

Final Equations for Parallel-Series L-Network Design

With the equations in their current form, **Eqn (13)** for X is a function of B, and thus B would need to be calculated before calculating X. We can remove the X's dependency on B by substituting each of the two versions of **Eqn (14)**, one at a time, for B in **Eqn (13)** and solving for X. Each equation for B will therefore have an associated equation for X.

The final results are two sets of equations, each set consisting of an equation for B and an associated equation for X, and each equation solely a function of Z_0, *Rload*, and *Xload*.

Each set of B, X equations represents a unique Parallel-Series L-Network solution. Thus, the two sets of equations represent two unique Parallel-Series L-Networks. These equations are listed below for the condition

$Rload \le Z_0$:

First Parallel-Series L-Network:
Shunt Susceptance:

$$B_1 = (1/Z_0)\sqrt{(Z_0 - Rload)/Rload}$$

Series Reactance:

$$X_1 = \sqrt{Rload\,(Z_0 - Rload)} - Xload$$

Second Parallel-Series L-Network:
Shunt Susceptance:

$$B_2 = -(1/Z_0)\sqrt{(Z_0 - Rload)/Rload}$$

Series Reactance:

$$X_2 = -\sqrt{Rload\,(Z_0 - Rload)} - Xload$$

In the special case in which $Rload = Z_0$ the two Parallel-Series L-Networks reduce to a single series reactance with no shunt component.

Final Equations for Series-Parallel L-Network Design

Similarly, note that **Eqn (20)**, the equation for B, is a function of X, and thus X would need to be calculated before calculating B. We can remove the B dependency on X by substituting each version of **Eqn (21)**, one equation at a time, for X in **Eqn (20)** and solving for B. Each equation for X will therefore have an associated equation for B.

The final results are two sets of equations, each set consisting of an equation for X and an associated equation for B, and each equation solely a function of Z_0, *Gload*, and *Bload*. *Gload* and *Bload*, themselves, are solely functions of *Rload*, and *Xload*.

Each set of X, B equations represents a unique Series-Parallel L-Network solution. Thus, the two sets of equations represent two unique Series-Parallel L-Networks. These equations are listed below for the condition $Gload \le 1/Z_0$:

First Series-Parallel L-Network:
Series Reactance:

$$X_1 = Z_0\sqrt{(1/Z_0 - Gload)/Gload}$$

Shunt Susceptance:

$$B_1 = \sqrt{Gload\,(1/Z_0 - Gload)} - Bload$$

Second Series-Parallel L-Network:
Series Reactance:

$$X_2 = -Z_0\sqrt{(1/Z_0 - Gload)/Gload}$$

Shunt Susceptance:

$$B_2 = -\sqrt{Gload\,(1/Z_0 - Gload)} - Bload$$

where:

$$Gload = \frac{Rload}{Rload^2 + Xload^2}$$

$$Bload = -\left(\frac{Xload}{Rload^2 + Xload^2}\right)$$

Note that in the special case in which $Gload = 1/Z_0$: the two Series-Parallel L-Networks reduce to a single component: a shunt susceptance.

Table 1 – Duality between the two networks.

New Series-Parallel	*Parallel-Series*
Eqn (20)	Eqn (13)
Eqn (21)	Eqn (14)
Eqn (23)	Eqn (16)

Determining Component Type and Calculating Component Values given *B* and *X*

The signs of B and X identify the types of component (inductor or capacitor) that B or X represents. Given a frequency F (in Hz), we can also calculate the values of those components:

- If B is negative, the component will be a **shunt inductor**, where, $L = -1/(2\pi F \cdot B)$.
- If B is positive, the component will be a **shunt capacitor**, where, $C = B/(2\pi F)$.
- If X is negative, the component will be a **series capacitor**, where, $C = -1/(2\pi F \cdot X)$.
- If X is positive, the component will be a **series inductor**, where, $L = X/(2\pi F)$.

Thus, the signs of B and X in each of the two B, X pairs will determine what forms the Series-Parallel or Parallel-Series L-Networks can take.

For a Series-Parallel L-Network, the choices are (see **Figure 8**):
- (–X, –B) Series capacitor, shunt inductor (CsLp)
- (–X, +B) Series capacitor, shunt capacitor (CsCp)
- (+X, –B) Series inductor, shunt inductor (LsLp)
- (+X, +B) Series inductor, shunt capacitor (LsCp)

For a Parallel-Series L-Network, the choices are (see **Figure 9**):
- (–B, –X) Shunt inductor, series capacitor (LpCs)
- (–B, +X) Shunt inductor, series inductor (LpLs)
- (+B, –X) Shunt capacitor, series capacitor (CpCs)
- (+B, +X) Shunt capacitor, series inductor (CpLs)

An Example of the Calculations

Let's say that *Zload* = 40 + *j*50 Ω at 10 MHz, and our goal is to transform *Zload* to a Z_0 of 50 Ω, looking into the Input Port of the L-Network.

From *Zload*, by inspection:

- *Rload* = 40
- *Xload* = 50

Therefore, we can calculate:

- $1/Z_0 = 0.02$
- *Gload* = 0.00976
- *Bload* = -0.0122

Next, checking our criteria for selecting a Series-Parallel or a Parallel-Series L-Network:

Is *Rload* ≤ Z_0? 40 < 50, therefore the Parallel-Series criteria **passes**.

Is *Gload* ≤ $1/Z_0$? 0.0098 < 0.02, therefore the Series-Parallel criteria **passes**.

Because both selection-criteria pass, we can implement this impedance-transformation with either a Series-Parallel or a Parallel-Series L-Network. Calculating the *B*, *X* pairs for each results in four realizable L-Network options:

- Series-C, Parallel-C (CsCp)
- Series-L, Parallel-C (LsCp)
- Parallel-C, Series-C (CpCs)
- Parallel-L, Series-C (LpCs)

The *B* and *X* values for each of these networks, as well as their associated component values, are tabulated in **Figure 11**.

These four L-Networks, with component values, are shown in **Figure 12**. Note that the calculated component values for all four networks have been verified with *SimSmith* **[10]**.

Conclusion

This article presents L-Network equations that are solely a function of *Rload*, *Xload*, and Z_0 (Z_0 is a real, not complex value), that will transform any complex load impedance (whose real component is not negative) to Z_0.

This article also presents an alternate method for deriving the equations for a Series-Parallel L-Network in which the Load and Input Impedances are instead expressed as admittances, which significantly simplifies the derivation of these equations.

Finally, this article corrects the guidelines commonly used to determine if a Series-Parallel configuration or a Parallel-Series configuration should be used to transform a particular load impedance to Z_0, and points out that for many load impedances the selection of one L-Network configuration is not exclusive of the other.

Jeff Anderson, K6JCA, first licensed as WN6AHL in 1970 while a freshman in high school, upgraded to General class (WA6AHL) shortly thereafter, and much later to Amateur Extra class. He graduated from the University of California, Berkeley, with a BSEE in 1977 and began working as a hardware design engineer in Silicon Valley, designing digital and analog hardware for high-resolution graphics displays, video compression, packet networks, video post-production equipment, and echo-cancelling speakerphones. Now retired, Jeff continues to design, for fun, rather than profit. When not splitting and stacking wood for his wife he can usually be found lying on the couch, reading a book.

Parallel-Series Calculations						
		Calculated Value	Indicated Component	Equivalent X (ohms)	Component Values at 10 MHz	
First B, X Pair	B1	0.01	cap (Cp)	-100	1.59E-10	Farads
(CpCs)	X1	-30	cap (Cs)	-30	5.31E-10	Farads
2nd B, X Pair	B2	-0.01	ind (Lp)	100	1.59E-06	Henries
(LpCs)	X2	-70	cap (Cs)	-70	2.27E-10	Farads

Series-Parallel Calculations (admittance method):						
		Calculated Value	Indicated Component	Equivalent X (ohms)	Component Values at 10 MHz	
First B, X Pair	B1	0.02219215	cap (Cp)	-4.51E+01	3.53E-10	Farads
(LsCp)	X1	51.2347538	ind (Ls)	5.12E+01	8.15E-07	Henries
2nd B, X Pair	B2	0.0021981	cap (Cp)	-4.55E+02	3.50E-11	Farads
(CsCp)	X2	-51.2347538	Cap (Cs)	-5.12E+01	3.11E-10	Farads

Figure 11 — Four L-Networks that transform *Zload* = 40 + *j*50 Ω at 10 MHz to 50 Ω.

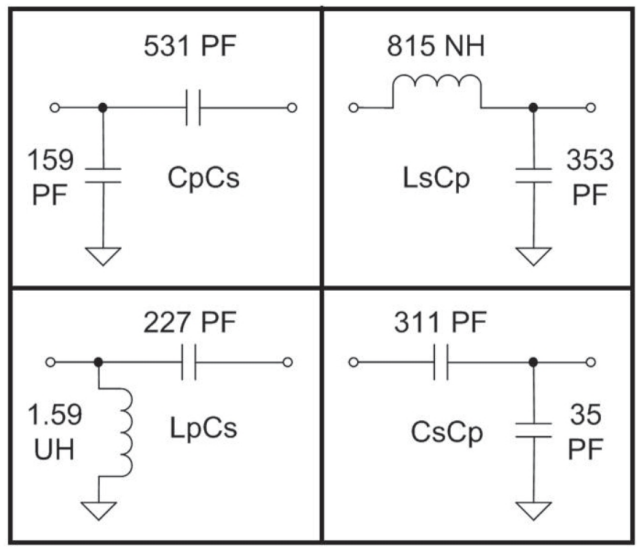

Figure 12 — The four L-Networks that convert *Zload* = 40 + *j*50 Ω at 10 MHz to 50 Ω. Because *Rload* satisfies *both* selection criteria, *Zload* can be transformed to 50 Ω with either one of the two Parallel-Series networks or with either one of the two Series-Parallel

Notes

[1] *The ARRL Handbook for Radio Communications*, ARRL, 2017, Figures 20.9A through 20.9D.
[2] D. Pozar, *Microwave Engineering, Second Edition*, Wiley, 1997, Figure 5.2.
[3] Page 4 of 26 in **https://uspas.fnal.gov/materials/10MIT/Lecture11.pdf**.
[4] H. W. Silver , NØAX, "Hands-On Radio, Experiment #61 – Smith Chart Fun III," *QST*, Feb. 2008.
[5] D. Pozar, *Microwave Engineering, Second Edition*, Wiley, 1997,. Eqns 5.1 through 5.3b.
[6] **https://k6jca.blogspot.com/2018/09/l-networks-new-equations-for-better.html**.
[7] D. Pozar, *Microwave Engineering, Second Edition*, Wiley, 1997. Page 230: "Note that since $R_L > Z_0$, the argument of the second square root is always positive."
[8] Page 4 of 51 in **https://my.ece.msstate.edu/faculty/donohoe/ece4333notes5.pdf**.
[9] Page 6 of 12 in **www.ittc.ku.edu/~jstiles/723/handouts/L%20Network%20Analysis%20present.pdf**.
[10] **www.ae6ty.com/smith_charts.html**.

Ron Block, NR2B
327 Barbara Dr., Clarksboro, NJ 08020; **ron@wrblock.com**

Single Point Ground Panel Location

A look at the significant issues that are faced in choosing the best location for a ground panel.

Since the publication of "Lightning Protection and Grounding Project at W2MMD" in the July 2022 issue of *QST*, I have had numerous questions regarding the placement of the protectors and whether they should be outside or inside the structure. It is not a simple decision and has many factors to consider. Below are some of the significant issues that we face in choosing the best location based on our individual circumstances.

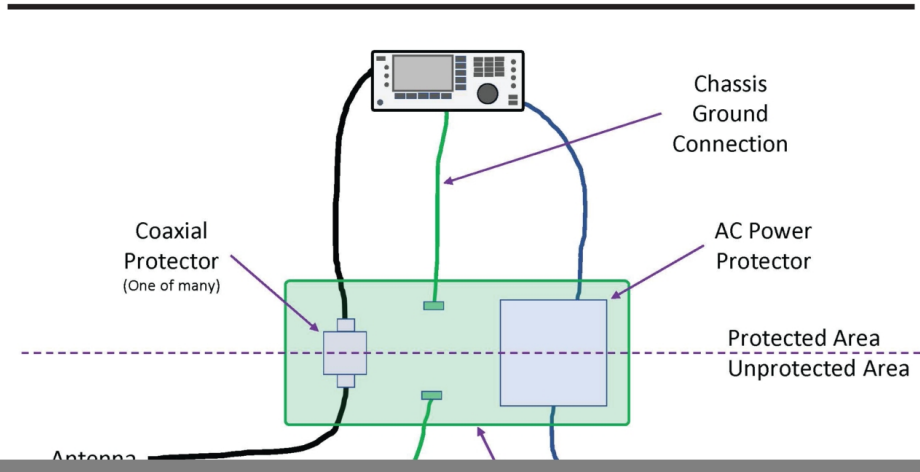

It's About "Time"

Let's first digress just a little to understand what the protectors do and why they need

any metal (copper, steel, aluminum) and in just about any shape that mechanically and electrically holds *all* of the protectors (coax, rotator, and ac-power) for the radio station. It also provides a convenient ground point for the equipment chassis. Protector layout (mechanical inter-protector spacing) can become an issue in some situations where there is a need, probably driven by radio equipment layout, to spread out the connections to accommodate various pieces of equipment. For proper operation, all protectors need to experience the surge energy at approximately the same time (within nanoseconds). This places some limits on where the protectors are placed with respect to each other. For every foot of separation between protectors, approximately a nanosecond is added before the protector is even aware of the surge energy. This delay, when combined with the normal 40 to 100 ns turn-on delay of the individual protector, must be short enough to limit the current flow on the yet to be short-circuited conductors. Depending on the design of the radio equipment interface circuitry, some soft damage could begin in as little as the seventy-five nanoseconds.

Now that we have an appreciation for the SPGP and the critical function that the protectors perform, let's examine where to place our SPGP.

Through-the-Wall

The best place for the SPGP is literally through-the-wall — a portion of the wall is removed and the panel is installed in its place — providing easy access from both the outside and the inside as shown in **Figure 2**. There are even special through-panel coaxial protectors that will mount directly on the SPGP and provide connector access to both sides. Additionally, this location usually facilitates a direct, short, and straight ground system connection and conveniently allows the use of wide, 2 to 6-inch or more, copper strap for a low inductance connection. This through-the-wall technique is employed successfully in commercial installations where the building's interior environment is intended for equipment and not necessarily for human comfort.

The problem for the amateur radio operator is cutting a hole in the side of the building sufficiently large to provide enough surface area to mount all of your coaxial, rotator, and ac-power protectors plus provide for future expansion. Since most stick-frame constructions uses 16-inch on-center spacing, the hole is approximately 16-inches by 1 to 3-feet. A hole this size may affect the future value of the property. The other, possibly more overriding concern is that the exposed thermally conductive metal of the SPGP will allow condensation, even ice, to accumulate on either side depending on the humidity and temperature difference. The condensation will eventually roll off the panel and onto the surrounding structure, which is probably not designed for a constant supply of water and thus encourages mold and rot. Thus, this optimal arrangement is not generally practical for hams.

Outside the Structure

If through-the-wall is not practical, then the next best place might be just on the outside of the structure where the coax cabling enters the structure, see **Figure 3**. This is a very popular and a logical place from a safety standpoint – keep most of the surge energy outside. The issue here is that *all* protectors (coax, rotor, and ac-power) need to be mounted on a common surface, in close proximity to each other, as we have discussed above. This is relatively easy for the coax and rotor protectors, but is more difficult when the ac-power protector is considered. Remember that the requirement to mount all of the protectors close to each other is to ensure that they each experience the surge energy overvoltage at about the same time.

Mounting the ac-power protector outside with the coax and rotor protectors presents an interesting mechanical and electrical challenge. The unprotected ac-power going to the ac-power protector most likely originates within the structure and must therefore exit the structure, go through the ac protector where it becomes protected, and then the protected ac-power must re-enter the structure and be distributed as the only source of ac power for the equipment.

That sounds easier than it is. The unprotected ac power leaving the structure and the protected ac power reentering the structure need to be physically separated by about a foot to prevent the potential for flash-over between the cabling. A flash-over would defeat the protection scheme. This is cumbersome, necessary, and doable only with some difficulty.

In addition, if one power protector doesn't provide the required current or voltage required by the equipment, then multiple power protectors will be necessary. Here, the protected cabling from multiple ac-power protectors may be bundled together and, separately, the unprotected cabling may be bundled together, while maintaining the protected / unprotected separation.

Don't lose sight of the need to provide weather protection for the protectors; most are not waterproof.

As an alternative in some very specific instances, it is possible to mount the ac-power protector inside on a mini SPGP and bond it to the outdoor coax and rotor protectors using a short, straight, wide (low inductance) copper strap. The length of the copper strap should be under five or six feet to keep the timing within the safety area. Keep in mind that a longer bonding conductor, multiple bends in the conductor, or a less-wide copper strap all add to the inductance and correspondingly add to the timing delay.

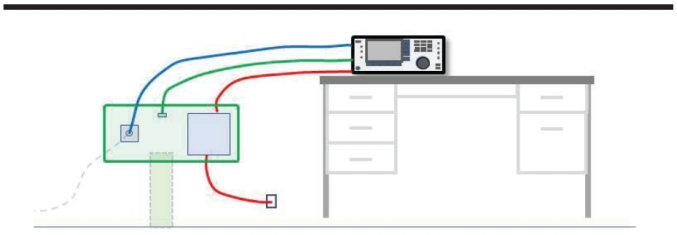

Figure 2 — Through-the-wall SPGP showing the inside view. The outside connections are shown as faded with dashed lines.

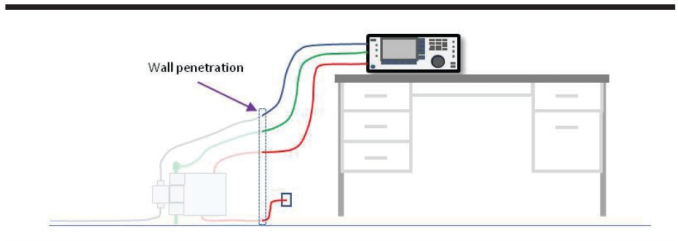

Figure 3 — The SPGP mounted immediately outside of the radio room with a separate exit and re-entry for the ac-power. Weather protection will most likely be necessary.

Inside the Structure

An alternative to putting the protectors outside the structure is to place the SPGP at a convenient mechanical and electrical point inside the structure along the path between where the cables enter the room and the radio equipment, see **Figure 4**. This interior location does allow the surge energy to enter the structure before it is rerouted back outside into the ground system. This increases the importance of having a low impedance path to the ground system, preferably interconnected with low inductance copper strap. The biggest challenge with this alternative is getting a multi-inch wide copper strap through the wall and to the ground system. This is particularly difficult for upper floors in a building; so much so that it needs to be covered as a separate future topic.

One way to improve your protection system and also lower the amount of surge energy coming to the SPGP is to incorporate radials at the base of each antenna support. The radials will allow surge energy that originates at the antenna to be dissipated into the earth leaving less energy to follow the coax cables to the SPGP. This is the plan for the W2MMD project; see "Lightning Protection and Grounding Project at W2MMD" in the July 2022 issue of *QST*. In addition, we will be creating a Perimeter Ground to both equalize the ground voltages beneath the Club House and to interconnect the utility and numerous freestanding antenna grounds. The Perimeter Ground will also interconnect with the radials on each of the towers to electrically bond the entire system together thereby enhancing the ground connection and improving RF performance. I expect that most of the surge energy (>60%) will be dissipated outside the Club House with the remainder following the cabling inside.

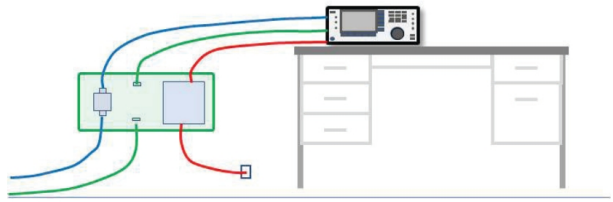

Figure 4 — The SPGP with protectors mounted inside the radio room along the physical coax cable path.

Interior Room

Up to now, we have been talking about the primary set of protectors; the ones for which proximity to each other is critical. For those radio installations that are located well within the structure (no outside wall) or that have cabling traveling through the structure for some distance (>25 feet), it may be advisable to install a secondary set of coaxial and rotor (not power) protectors at the cable entrance to remove some of the energy from the cables before they traverse the interior of the structure. The secondary protectors are there to minimize flashover to the structure along the cable path by removing some of the surge energy; they are not there to provide protection for the radio equipment.

Wrap-up

One more point. Be aware that a whole house type surge protector, installed at or near the main distribution panel, has no effect on the design or deployment of the SPGP and the protection that it provides. While it will offer some level of protection to household electronics, it is almost always too far away from the SPGP to be timely. In the very rare case where it comes close to meeting the timing requirement, the SPGP surface may be extended using wide copper strap to include it as the ac-power protector.

These are your top-level choices along with the major difficulties and advantages. Every situation is unique and will present numerous other challenges that need resolution. Just keep the door knob concept in mind and your variations should be good.

For additional information consult *Grounding and Bonding for the Radio Amateur*, Second Edition, by H. Ward Silver, NØAX, and "Lightning Protection for the Amateur Radio Station" by Ron Block in the June, July, and August 2002 issues of *QST*.

ARRL member Ron Block, NR2B, holds an Amateur Extra class license. He worked for twenty years in the computer industry as a project manager for complex one-time computer-based projects. In parallel he became a PolyPhaser distributor and consulted extensively in lightning protection and grounding. He is also the brother of the late PolyPhaser Corporation founder, Roger R. Block, KD7UT.

H. Lawrence Serra, N6NC
1135 Torrey Pines Rd. Apt. 2C, La Jolla, CA 92037; **hlserra@gmail.com**

Make-Do Ham Interferometer to Determine Elevation Angles of Arriving RF Signals

Confirm the correlation between VOACAP take-off angles and received angles of arrival with a make-do interferometer.

In order to confirm the correlation between VOACAP take-off angles (TOA) and received angles of arrival (AOA) for a trans-North Pacific propagation investigation **[1]** I guessed I had enough equipment to create a make-do interferometer. This would enable me to determine the received AOAs at my San Diego QTH to compare them with the TOAs of various HF shortwave stations located in Japan, along the Asian coast, Oceania, Cuba, Florida, North and South Carolina, and WWV/WWVH. I found an article online **[2]** that determined the phase angle between voltages by dividing difference of the times of arrival of two voltages by their period.

Then I discovered that my PAØRDT mini-whip active antennas had been modeled by VK1OD and that the profile of the antenna was basically a monopole vertical whose radiation pattern is shaped like an inverted stemless champagne flute with its peak at the top elevation of the antenna pod.

Another ham had created a rough correlation table for the PAØRDT antenna between the phase angle of the voltage of the received wave (between 0° to 300°) and the received elevation angle of arrival (AOA) of that signal between 10° and 40°. My testing extended the correlation table downward to –50° phase angle (= 5° AOA) and –60° phase angle (= 4° AOA).

Years earlier, I had obtained a used Rigol DS1102E digital two-channel 100 MHz oscilloscope. When I was doing simple RF wave shape examinations I had noticed that the scope displayed a table of numerical calculations. It occurred to me, and the manual confirmed, that the measurement functions of the scope would provide the frequency, period, and the difference between times of arrival of the two antennas.

The articles I had read on determining elevation angle talked about wide-spacing of the two antennas; one antenna must go to scope Channel A, the other to scope Channel B. Then the arrival time of the same signal at each antenna could be compared to produce the time delay between them, which divided by the period of the wave, would produce the phase angle of the wave. Then I would compare the phase angle on the correlation chart to the calculated elevation angle of arrival (AOA) of the PAØRDT antennas.

The antennas were separated by only 37 feet horizontally and 20 feet vertically in my suburban village environment, so I was concerned I might not have enough antenna spacing. In his article on elevation arrival angles **[3]**, K9LA used two Yagis separated at greater distances both vertically and horizontally. Of course, with two vertical antennas I lose the ability to confirm azimuth direction of the signal, but from a year as an SWL before becoming licensed I knew how to track down the transmitter locations of various HF shortwave stations. This online locator **https://www.short-wave.info/index.php** makes it even easier today.

Interestingly, the digital scope measured delay down to nanoseconds difference, which proved to be enough to record and measure the delay interval between arrival times of the signal from each antenna.

I learned to measure the length of the coaxial cable runs in order to establish the latency delay times caused by the velocity of the cables, and to remove those delays from the time of arrival of each antenna recorded by the measuring oscilloscope. It turns out that's easily done. The delay times of the most used coaxial cables are available online and easily determined, see: **https://studylib.net/doc/18203254/calculating-the-propagation-delay-of-coaxial-cable**.

The phase angle is given by:

$$\Phi = 360 \times td \,/\, tp$$

where *td* is the Δ time of arrival between the two antennas, and *tp* is period of the wave multiplied by 360°.

One antenna is connected to CH-A and one to CH-B, and the scope compares the arrival times of the two antennas and displays the Δ time between the two for a general comparison. For more precision, I subtract the coaxial delay from each Channel's reported arrival time, then take the difference of time between those latency-adjusted arrival times. That difference in time is divided by the period of the wave reported by the scope, and produces a decimal number that when multiplied by 360° produces the phase angle of the received signal. Here's an example:

The phase angle is

$$\Phi = 360° \times 10 \text{ ns} \,/\, 100 \text{ ns} = 36°.$$

That phase angle number is compared on the correlation table for the PAØRDT

Table 1 – Phase Angle to Angle of Arrival

PH	*AOA*
< 300°	40°
< 200°	30°
< 100°	20°
< 0°	10°
< –50°	5°
< –60°	4°

antenna to determine the angle of arrival (AOA). **Table 1** is a correlation table developed by another ham and modified by me to add data from low and negative phase angle measurements.

I ran various tests on numerous HF shortwave stations from September through November 2021, including Radio Japan, Radio Taiwan, Radio Thailand, Radio New Zealand, Radio Havana, both WWVs, Russian Nuclear Forces beacons, and US shortwave stations transmitting from Florida and North and South Carolina. A receive antenna is constantly receiving wave signals at various angles of arrival (AOA), and the take off angle (TOA) of the strongest signals reported by VOACAP for each station correlated to within 0° and 2° of my interferometer angle of arrival. This makes common sense when you think about it. The physics of long-range signal refractions and reflections being what they are, the strongest signals produced by the transmitting antenna TOA will likely be the strongest signals received by the receiver antenna, plus or minus some minor refracted differences, barring any ionospheric anomalies like TIDs (traveling ionospheric disturbances), 500 mB wind shear (Jetstream) disturbances, massive cyclones like hurricanes, typhoons, towering mid-continent thunderstorms, and weather-front induced gravity waves, all of which can ripple or disturb the ionosphere and cause anomalous propagation effects. I contend that it is highly unlikely you will receive a 30° strongest AOA when the strongest wave of the DX transmitter TOA is at 8°.

The biggest problem on my particular scope is that I'm at the foot of Mount Soledad in San Diego, which contains commercial and Navy transmitter sites so there is a constant barrage of different frequencies displaying different periods on the scope, even with the addition of broadcast band filters to each reference antenna. So it takes a little bit of patience and adjustment to stabilize the scope's reporting to get the proper frequency and period of the reference signal. Nonetheless, the results were encouraging and prompted me to continue my investigation of the July 24, 2010 recording of 141 JA call signs by my CW skimmer.

Table 2 – N6NC AOA compared with VOACAP TOA, deg.

Date/time		*AOA*	*TOA*
9/22/21	WWV 10MHz Boulder CO Radio Beijing 15160kHz		
0615Z		25	25
9/27/21	Radio Thailand 15590kHz Bangkok		
0040Z		11	10
9/28/21	Radio Havana 15370kHz Havana		
2215Z	(Mt Soledad masks low-angle calculated path)	40	12
2245Z		13	10
9/28/21	KNX 1070AM Los Angeles 1070kHz Torrance CA (Heavy Marine layer along coast; ground wave and sky wave)		
1846Z		19	10
1901Z		10	10
1915Z		11	10
9/29/21	Radio Beijing 15160kHz		
0320Z		16	5
0330Z		10	5
0415Z		11	9
9/29/21	Radio New Zealand 15725kHz (Rangitaiki, North Island NZ)		
1030Z		11	9
1100Z		8	9
1130Z		7	6
9/29/21	RADIO BEIJING 15160kHz		
0415Z		11	9
9/30/21	WWV 10MHz Boulder CO		
2140Z		21	21
10/16/21	WWV 10MHz Boulder CO		
2245Z		17.6	17
2245Z-2300Z		14.33	14
10/17/21	WWV 10MHz Boulder CO		
0001Z		12.7	14
10/17/21	WWV 10MHz HI		
1706Z		13	14
10/17/21	WWV 10MHz Boulder CO		
1800Z		18	16
1900Z		14.9	14
2000Z		17.2	19
10/21/21	WWVH 10MHz HI		
2300Z		12	13
10/22/21	WWVH 10MHz HI		
0315Z		17.7	18
10/22/21	WWV 5MHz Boulder CO		
0340Z		39	41
10/23/21	WWV 10MHz Boulder CO		
1615Z		15	14

Here is the step by step procedure to record AOAs to compare with VOACAP TOAs.

1) With a digital calculating/recording oscilloscope, two antennas, simple tuners, two SDRs, and some math you can calculate the elevation angle of arrival of RF signals.

2) The formula for the PHASE angle of arrival of an RF signal is pretty simple, and from it you can correlate from PHASE Angle to Elevation Angle of Arrival of the signal at your antennas.

$$\Phi = 360 \times td / tp = \text{PHI}$$

td = time delay between the signals arriving at each antenna

tp = period of the signal.

3) Tune each SDR on its own antenna to the signal in question. If possible the antennas should be more than one wavelength apart, with their axes perpendicular to the signal path, and at different heights, but closer spacing works too.

4) Tune the mini-tuner of each antenna to peak the signal. I've added two identical preselectors to amplify the antenna signals, and two identical BCI filters, each with negligible measured latency delay.

5) To avoid the substantial, nearly incalculable latency SDRs delays, switch the tuned antennas off the SDRs and connect them directly to the CH-A and CH-B inputs on the scope. Adjust the scope to size the signals and engage the scope's cursors and Measurement (calculation) functions.

6) Either with automatic or manual cursor tracking, find the delay time between the arrivals of the signal at each antenna (usually in µs or ns range), and the period of the signal. Keep your units straight!

7) Ballpark the latency delay of your coax runs to the two antennas. You can determine the coax lengths with a tape measure, or directly if you have an antenna analyzer.

Date/time		*AOA*	*TOA*
10/23/21	WRMI 15770kHz Okeechobee FL		
1745Z		12	11
1846Z		12	11
10/23/21	WRMI 21525kHz FL		
1915Z		18	16
10/24/21	WWV 10MHz		
1700Z		14.8	14
10/24/21	WWCR 12160kHz Nashville TN		
1723Z		16.3	18
10/30/21	WWV 20MHz Boulder CO		
2130Z		22.5	21
11/03/21	SuperDARN HF Radar 11070kHz Hokkaido Japan		
1635Z		11	12
		11.5	12
1830Z		11.15	12
11/05/21	Russian Strategic Nuclear Forces Beacon "F" 7040kHz Vladivostok		
1500Z		10.4	10
11/05/21	Radio Taiwan 7300kHz		
1530Z		11.8	10
11/05/21	Radio Marti 13820kHz Greenville NC		
1830Z		17.2	17
11/05/21	WHRI 21610kHz Cypress Creek SC		
1900Z	(Mt Soledad blocks low angles from east)	11.6	8
11/05/21	Radio New Zealand 11690kHz (North Island)		
1903Z		9.1	10
11/06/21	KNX 1070kHz AM Torrance CA		
0030Z		17.2	17
11/13/21	WWV 10MHz Boulder CO		
2230Z		10.7	8
11/14/21	WWV 20MHz Boulder CO		
0130Z		13	15
0220Z		16.3	15
11/16/21	WWV 10MHz Boulder CO		
1815Z		12	10
1845Z		10	10
1900Z		4	5
11/16/21	KNX 1070kHz AM Torrance CA		
1915Z		6	5
2107Z		17	21
2205Z		8	4
11/16/21	WWV 10MHz Boulder CO		
2300Z		6.5	8
11/17/21	Radio Havana 15370kHz		
2130Z		7	8

You can find your coax delay in ns per foot here: **https://studylib.net/doc/18203254/calculating-the-propagation-delay-of-coaxial-cable**. Subtract these coax delay times from the times the scope shows for each antenna on CH-A and CH-B. The difference between the CHs adjusted delay times is the adjusted *td* for the formula.

8) Apply the adjusted delay time and the signal's period to the formula. If the quotient is a multiplier of a number, such as 3.427, subtract the ones digit from the number, (e.g., 3.427 – 3 = 0.427) and use that result to multiply by 360°. This manipulation removes the multiple 360°/2π cycles that the scope's measuring device might have included depending upon the time base you have chosen.

9) Use the result to multiply by 360°, and the formula gives you the PHASE Angle of the signal. If the resulting PHASE Angle seems implausibly high after calculation, subtract another 360° from it, which might reduce it to a negative phase angle. This often happens with elevation AOAs below 10°.

10) Find the correlation table for your antennas' phase angles and elevation arrival angles or create such a table by comparing the received signal's elevation angle of arrival to the calculated elevation take off angle (TOA) in VOACAP through the ham interfaces of Jari Perkiömäk, OH6BG, **www.voacap.com/hf/** and Alex Shovkoplyas, VE3NEA, DX Atlas **www.dxatlas.com/download.asp** HAMCAP 1.91 interfaces. For any month, time and frequency, VOACAP shows the transmitter's probable elevation Take Off Angle (TOA) of an RF signal between two geographic points on the globe. From this data you can create your own correlation table between your antennas' PHASE Angle and Elevation Angle of Arrival (AOA), or use the EZNEC model of your antennas to determine the vertical gain profile of your antennas.

I've tested this method using two PAØRDT active antennas only 42 ft apart and separated in height by only 20 ft. It has produced adequately accurate results (± 2°) on most signals.

The purpose of the investigation is to find the elevation arrival angles in San Diego of Asian coast trans-Pacific signals to determine by geometry the last F2 layer refraction points and any sea surface reflection points along the path, which gives us a good idea where the middle hop — from ocean to ionosphere back to ocean — likely occurred.

Table 2 shows some examples of recorded N6NC AOAs compared to VOACAP TOAs. For a few of these records I used the adjusted Phase Angle formula to reduce each antenna's time of receipt by its coax delay, but for most entries I simply used the Phase Angle formula unadjusted for coax delay because the difference in angle reports was miniscule .

HL Serra, N6NC, has been a licensed amateur since 1959. He has held a USCG Master's license, served in the US Merchant Marine (1964-65) and the US Navy (1968-70) as an OOD, navigator and naval intelligence officer in Vietnam and Cambodia. He has sailed the Atlantic and Pacific Oceans, the Caribbean Sea, sailed to all the countries of the Western Pacific Rim, transited the Pacific from Japan to San Diego, and transited the Panama Canal. In 2009-2011 he quarterbacked the successful legal defense of San Diego radio amateurs against a proposed ordinance intended to prevent the erection of HF antennas in the City of San Diego. His strategy was adopted by the ARRL and serves as the template for defense against similar local measures. He retired as a practicing lawyer and law professor in 2013, and in 2016 earned a masters degree from Scripps Institution of Oceanography/UCSD, with an interest in the physical causes of meteorological and climate events. He has published articles in QST *and* NCJ *on antennas that he designed and built, and he assembled and captained the 6E2T contest team that won the 1995 ARRL DX CW Contest (DX WORLD M/2 class) from Ensenada, Mexico. Since then he contests with the NX6T team remotely to the WA6TQT Anza Radio Ranch contest station.*

References

[1] H. Lawrence Serra , N6NC, "Why Summer 40 m Propagation Is So Good Between Japan and the US Pacific Coast," *QEX* ARRL, Sep./Oct. 2022, pp. 14-18.
[2] **https://www.edn.com/measure-phase-difference-with-an-oscilloscope/**.
[3] C. Luetzelschwab, K9LA, "Measuring the Elevation Angle of Arriving Signals," Propagation: *WorldRadio*, Dec. 2013.

Wojciech Kaczmarski, SP5WWP and **Jay Francis, KA1PQK**

Partyzantow 16/13 Nowy Dwór Mazowiecki, PL 05-100, Poland; **w.kaczmarski@teletra.pl**

4 Klara Dr., Merrimack, NH 03054; **ka1pqk@arrl.net**

Designing a Square Root Nyquist Filter for a Modern Digital Radio Protocol

Abstract

The Parks-McClellan method is used to design optimized square root Nyquist filters that are better at reducing intersymbol interference in digital communications than legacy root raised cosine filters. These optimized filters can perform better while retaining the same filter order as the legacy filter, or perform similarly while reducing the filter order. A metric to evaluate intersymbol interference of a given square root Nyquist filter is established. A MATLAB program is used to search the design space to obtain an optimized root raised cosine filter and two optimized Parks-McClellan filters with features applicable to the *M17 Project* radio protocol.

1 Introduction

Filters that meet the Nyquist condition for zero intersymbol interference (ISI) play an important role in digital communications [1]. In order to meet the condition, the overall time domain channel transfer function (transmitter to receiver) must not allow other symbol values to influence the current symbol's value at the time it is sampled. If the sampling point is at $t = 0$, we can picture prior (and future) symbols occurring at intervals of kT ($k \in \mathbb{Z} : k \neq 0$) where T is the symbol duration. At $t = 0$, the channel transfer function should be exactly 1 (for a unity-gain function). At all other possible sampling points kT, the channel transfer function should be 0. At any other points in time, the function can have an arbitrary value. These conditions can be met by the transfer function of Eq. 1.

$$h(t) = \begin{cases} 1 & t = 0 \\ 0 & t = kT, \{k \in \mathbb{Z} : k \neq 0\} \end{cases} \quad (1)$$

In theory, there are an infinite number of solutions to this function. In practice, the frequency response $H(f)$ of the transfer function must also be taken into consideration [2]. The minimal bandwidth solution for $h(t)$ is of the form $\frac{\sin x}{x}$, with an $H(f)$ response of a low pass filter with cutoff at $\frac{1}{2T}$ and gain of T. Unfortunately, this is an unrealizable filter because the $h(t)$ response extends infinitely in time and does not converge. To help solve those problems, implementations will relax the transition taper of $H(f)$ while still transitioning through the -6 dB point at $f = \frac{1}{T}$, and truncate the $h(t)$ response, with a tradeoff in ISI performance due to $h(t) \neq 0$ where $t = kT$. Filters that are designed to meet the Nyquist condition for zero ISI are known as Nyquist filters.

Communication systems will split the implementation of the desired Nyquist filter transfer function across both the transmitter and receiver. Using $\sqrt{H(f)}$ as a filter at both the transmitter and receiver will result in an overall transfer function of $H(f)$. The matched filters in this case are called square root Nyquist filters. The square root operation does not affect the passband nor stopband gains, but does affect the taper such that the gain is -3 dB at $f = \frac{1}{2T}$ [2].

The raised cosine function (RC) and its related root raised cosine (RRC) functions are often used to construct approximations of Nyquist and square root Nyquist filters. As the name suggests, the taper function of the RC filter is

*SP5WWP, M17 Project founder and team lead, ARRL's Technical Innovation Award 2021 recipient

†KA1PQK, M17 Project team member, Open Research Institute contributor

the cosine itself. The frequency response at the transition band between $(1-\alpha)f_h$ and $(1+\alpha)f_h$, where $f_h = \frac{1}{2T}$, is given by Eq. 2. Otherwise, the response is a constant 1 at the passband ($0 \leq f \leq (1-\alpha)f_h$) and 0 at the stopband ($f \geq (1+\alpha)f_h$) [1].

$$H_{RC}(f) = \frac{1}{2}\left[1 + cos\left(\frac{\pi T}{\alpha}\left(f - \frac{(1-\alpha)}{2T}\right)\right)\right] \quad (2)$$

While the $H_{RC}(f)$ function appears smooth, the corresponding RRC filter taper $\sqrt{H_{RC}(f)}$ is not. The first derivative of this piecewise-defined frequency response function has a step at $(1+\alpha)f_h$ [2]. RRC filters suffer a performance limitation due to the presence of a sudden value change of the first derivative of their taper function.

In this work, finite impulse response (FIR) digital filters are utilized. These are discrete time filters with no feedback in the filter's topology [4]. For an N-tap FIR filter, the z-transform of the transfer function, $H_{FIR}(z)$, is given by Eq. 3.

$$H_{FIR}(z) = \sum_{i=0}^{N-1} b_i z^{-i} \quad (3)$$

The impulse response of an FIR filter returns its taps, the b_i terms, where $i = 0...N-1$ [4]. At a sampling rate of f_s and a symbol duration of T, we have $r = f_s T$ samples per symbol, and the filter is said to span $K = \frac{N-1}{r}$ symbols. By convolving the taps of a square root Nyquist filter with themselves, $c_i = b_i * b_i$, the resulting $c_i, i = 0...2rK$ values should be null at every r interval, except at $i = rK$ where the value is expected to be non-zero [3]. If the r interval values are not null, there will be some amount of ISI. Since the natural figure of merit for a Nyquist filter is its ability to minimize the ISI, the root mean square (RMS) of all $c_i, i = 0, r, 2r...2rK, i \neq rK$ values can used to form a cost function Eq. 4. The middle value $i = rK$ is excluded as it corresponds to the peak of the impulse response. With an established cost function, the ISI performance of multiple square root Nyquist filters can be compared.

$$RMS\,ISI = \sqrt{\frac{1}{2K}\sum_{i=0,r,2r...}^{2rK,i\neq rK} {c_i}^2} \quad (4)$$

The aim of the work presented in this paper is to find square root Nyquist filters for use in the *M17 Project* radio protocol [5]. First, an RRC filter is designed with parameters that minimize the RMS ISI. Then, two square root Nyquist filters are designed using the Parks-McClellan method [4]. One filter retains the same filter order as the RRC filter and parameters are adjusted to minimize RMS ISI, while the other filter's order is reduced along with adjusting paramters to minimize RMS ISI to the point where its RMS ISI is less than that of the RRC filter.

2 Methods

A MATLAB [6] script was used to perform all calculations and plot results [7]. Parameters were exhaustively searched using reasonable step sizes, initial, and final values.

The MATLAB function `rcosdesign` was used to obtain RRC filter taps across the search parameters. With the excess bandwidth coefficient α fixed at 0.5, the search considered span K ranging from 2 to 10 with a step size of 2, and samples per symbol r ranging from 2 to 10 with a step size of 1. Taps were convolved and the RMS ISI was calculated according to Eq. 4. The parameters and taps that resulted in the minimal RMS ISI were retained as the final RRC filter. Passband ripple and stopband attenuation were computed. To verify the square root Nyquist filter requirement of -3 dB at f_h, the magnitude of the response at f_h was determined.

The Parks-McClellan MATLAB function `firpm` was used to generate FIR coefficients for two square root Nyquist filters. The function parameters were the filter order, the frequency vector used to form frequency bands, the desired frequency response amplitude vector, and a weight vector which tells the algorithm how to adjust the fit of the frequency response.

Both filters used the samples per symbol r of the RRC filter. For one filter, Optimized, the span K of the RRC filter was kept, such that the filter order was held at a constant rK, the same filter order as the RRC filter. The second filter, Reduced Optimized, was allowed to search over lower spans in order to find a filter with similar performance to, but lower filter order compared to the RRC filter.

The frequency vector input for both filters is shown in Eq. 5. These five frequencies form three bands of a low-pass filter. The β_1 and β_2 terms were used to adjust the taper end points between the passband and stopband. β_1 ranged

from 0.1 to 1.0 at a 0.025 step size. β_2 ranged from 0.1 to $r-1$ at a 0.025 step size such that $(1+\beta_2)f_h \leq \frac{f_s}{2}$.

$$f_{pm} = \left[0, (1-\beta_1)f_h, f_h, (1+\beta_2)f_h, \frac{f_s}{2}\right] \quad (5)$$

The desired frequency response (gain) for both filters at these points were defined in Eq. 6. For frequencies below $(1-\beta_1)f_h$ the gain was unity, above $(1+\beta_2)f_h$ the gain was zero. At f_h, the gain of a square root Nyquist filter has to be equal to $\frac{\sqrt{2}}{2}$ (-3 dB by voltage).

$$A_{pm} = \left[1, 1, \frac{\sqrt{2}}{2}, 0, 0\right] \quad (6)$$

The weight vector Eq. 7 included the parameter γ that affected the passband weight of both filters and ranged from 0.1 to 10 with a 0.025 step size.

$$W = [\gamma, 1, 1] \quad (7)$$

Filter taps for both filters were were convolved and the RMS ISI values were calculated according to Eq. 4. The parameters and taps that resulted in minimal RMS ISI values were retained as the final Optimized and Reduced Optimized filters. Passband ripple and stopband attenuation were computed for both filters. To verify the square root Nyquist filter requirement of -3 dB at f_h, the magnitude of the response at f_h was determined for both filters.

A mismatched configuration of RRC and Optimized filters was considered by convolving filter taps of one filter with the other and calculating RMS ISI according to Eq. 4.

3 Results

An RRC filter with parameters $\alpha = 0.5$, span $K = 8$, samples per symbol $r = 10$, and RMS ISI = 3.8e-05 was found. An Optimized filter with parameters span $K = 8$, samples per symbol $r = 10$, $\gamma = 1.325$, $\beta_1 = 0.675$, $\beta_2 = 1.000$, and RMS ISI = 1.1e-05 was found. A Reduced Optimized filter with parameters span $K = 4$, samples per symbol $r = 10$, $\gamma = 6.800$, $\beta_1 = 0.725$, $\beta_2 = 1.000$, and RMS ISI = 3.6e-05 was found. The magnitude of the frequency response for all three filters is shown in Figure 1, with a zoomed in look at the passband ripple for all three filters shown in Figure 2. The c_i values used to compute RMS ISI in Eq. 4 are plotted for each filter in Figure 3. The number of taps, passband ripple, stopband attenuation, magnitude at f_h, and RMS ISI for each filter are shown in Table 1. The mismatched configuration of RRC and Optimized filters resulted in an RMS ISI of 2.3e-05.

All filters met the square root Nyquist filter requirement of passing through the -3 dB point at f_h. Examining the frequency response plots in Figure 1, one can see that the stopband performance of the RRC filter is the least desirable. Increased stopband attenuation results in more energy focused into the passband and better ISI performance. The Optimized filter had the lowest RMS ISI value, the least amount of passband ripple, and the best stopband attenuation. The Reduced Optimized filter, with half the filter order of the RRC filter, outperformed the RRC filter in passband ripple and stopband attenuation while maintaining a similar RMS ISI value. Even a mismatched system using RRC and Optimized filters should perform better than one with RRC filters only.

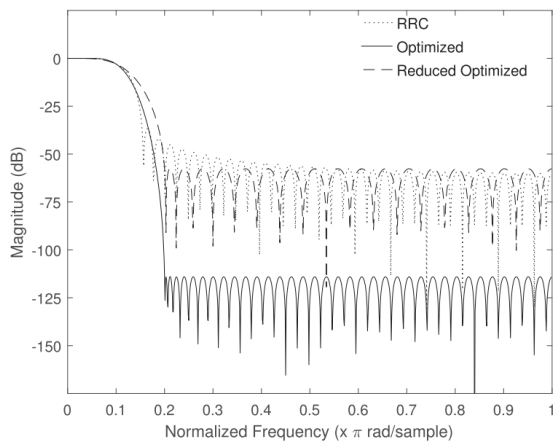

Figure 1: Overall frequency response of RRC, Optimized, and Reduced Optimized filters.

4 Discussion

The *M17 Project* is developing a fully open source digital voice and data protocol. Handheld communication transceivers such as the *TYT MD-380* [8], using open source firmware such as *OpenRTX* [9], are expected represent a large portion of M17's user base. This class of transceiver is built around low power microcontrollers that

Table 1: RRC, Optimized, and Reduced Optimized filter comparisons.

	RRC	Optimized	Reduced Optimized
Taps	81	81	41
Passband Ripple (dB)	8.5e-03	1.7e-05	2.4e-03
Stopband Attenuation (dB)	-27	-104	-55
RMS ISI	3.8e-05	1.1e-05	3.6e-05

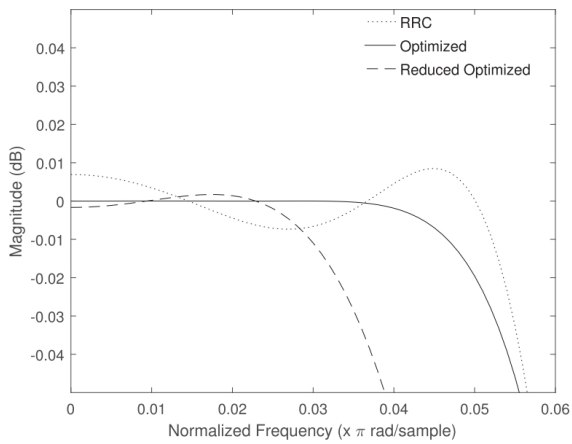

Figure 2: Passband ripple of RRC, Optimized, and Reduced Optimized filters.

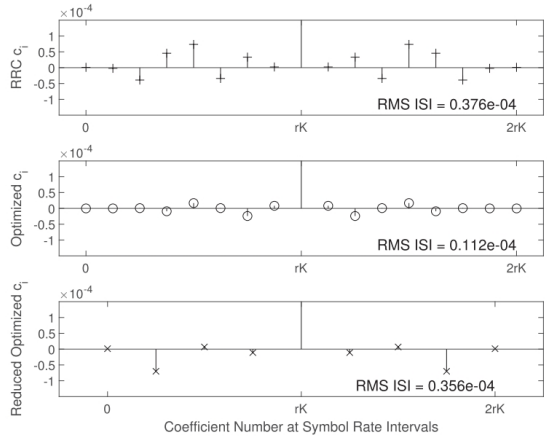

Figure 3: Intersymbol interference c_i values plotted for RRC, Optimized, and Reduced Optimized filters.

generally have limited compute and memory resources. Any performance gains, whether they provide better system performance while utilizing similar resources, or equivalent performance using fewer resources, are extremely important. In the case of a square root Nyquist filter used for ISI reduction and approximated with an FIR filter, the resources required are directly related to the number of taps. The work presented here has shown that the typical implementation of Nyquist filters using the legacy RRC approach is not as effective as the Optimized (better performance, similar resources) or Reduced Optimized (similar performance, fewer resources).

As the M17 protocol is developed, much of the processing burden falls on the microcontroller, which led to certain experimental design choices and tradeoffs in this work. Large volume established products can offload processing to dedicated hardware, as is often done with the Nyquist filter. An example of this is Analog Devices' ADF7021 narrow-band transceiver [10]. This highly intergrated device implements RRC filters, however, the choices of the roll-off factor α are limited to 0.5 or 0.7 in hardware. In preparation of for the work presented here, the MATLAB script to find the best RRC parameters was modified to search over different α values. We found a solution in the vicinity of $\alpha = 0.8$ but determined that this expanded the system bandwidth beyond what was acceptable for M17. Searching over the range starting at $\alpha = 0.7$ and lower, based on the values available in the ADF7021 which was being considered for M17 development, resulted in finding the best solutions with $\alpha = 0.5$. This was an experimental design choice, and certainly could be an area of future exploration.

Limiting the RRC filter search to a maximum filter order of 100 was another experimental design choice based on practical experience. Microcontroller implementations of M17 using RRC filters where the filter order was in excess of 100 were found to be very resource heavy and caused issues in other areas of processing. RRC filters will perform better as the filter order increases, and there may be cases where a higher order RRC filter has comparable performance to other filter designs. If compute resources are plentiful, expanding the search to higher order filters seems prudent.

When discussing expansion of the search space, one has to address the issue of the exhaus-

tive search method and step sizes used in this work. Given the numerous constraints placed on the search parameters, an exhaustive search was the most reliable method to use, assuming the step sizes were granular enough. As the search space is increased, more advanced search techniques may be required.

Finally, as was pointed out in [2, pg. 98], the extensive use of the RRC filter may simply be the result of an off-hand comment by Nyquist. As the move towards even more software centric radios continues, it's a good time to re-evaluate old assumptions and investigate other possibilities.

5 Conclusions

Using filter design algorithms such as the Parks-McClellan method along with appropriate search methods and evaluation functions, square root Nyquist filters can be found that are better solutions to reduce intersymbol interference compared to legacy root raised cosine filters. These filters perform better than root raised cosine filters while maintaining the same filter order, or perform comparably well with a much smaller filter order. Either solution provides benefits for modern digital radio protocols such as the one used in the *M17 Project*.

6 Acknowledgments

We thank all *M17 Project* and *OpenRTX* team members, and our fiscal sponsors *Open Research Institute* and *Amateur Radio Digital Communications* for their support. This work was inspired by *An Improved Square-Root Nyquist Shaping Filter* original paper, published by harris, Dick, Seshagiri and Moerder in *Proceeding of the SDR 05 Technical Conference and Product Exposition*, 2005.

References

[1] Proakis, J., & Salehi, M. (2008). *Digital Communications* (5th ed.). McGraw-Hill Higher Education. pp. 602-609

[2] Harris, F. J. (2021). *Multirate Signal Processing for Communication Systems* (2nd ed.). River Publishers. pp. 87-107

[3] Harris, F. J., Dick, C., Seshagiri, S., & Moerder, K. (2005). An Improved Square-Root Nyquist Shaping Filter. *Proceeding of the SDR 05 Technical Conference and Product Exposition.*

[4] Oppenheim, A. V., & Schafer, R. W. (1989). *Discrete-Time Signal Processing.* Prentice Hall. pp 212, 313-314, 476-480

[5] *M17 Project.* https://m17project.org

[6] *MATLAB R2022a* (2022). The MathWorks Inc. https://www.mathworks.com

[7] *rnyq_paper.m MATLAB script.* https://bit.ly/rnyq_paper

[8] *TYT MD-380 DMR two-way radio.* Quanzhou TYT Ekectronics Co., Ltd. https://www.tyt888.com

[9] *OpenRTX Project.* https://openrtx.org

[10] *ADF7021 High Performance Narrow-Band Transceiver IC Data Sheet* (2016, Rev. D). Analog Devices, Inc. https//www.analog.com

Wojciech Kaczmarski, SP5WWP, has been licensed since 2016. He has started the M17 Project in 2019. He received the ARRL's Technical Innovation Award in 2021. Wojciech works as a bare-metal and embedded software developer, electronic engineer, and hardware tester. In his free time, he enjoys reading mind-expanding science and philosophy books. He can be reached at Partyzantow 16/13 Nowy Dwór Mazowiecki, 05-100, Poland; w.kaczmarski@teletra.pl.

Jay Francis, KA1PQK, has been a ham since 1988, but grew up around his father's (K1PTF) radios and boxes of parts. Jay is currently a freelance hardware/firmware/software engineer working on projects ranging from robots to rockets. Before going freelance, he worked primarily as a hardware engineer designing network equipment. He holds master's degrees in Electrical Engineering and Exercise Science. When not working in the lab, you'll likely find Jay outside swimming, biking, or running. He can be reached at 4 Klara Dr., Merrimack, NH 03054; ka1pqk@arrl.net.

The SWR Circle

A Standing Wave Ratio (SWR) circle is the result of a few quick, grade-school math calculations that give insight as to the range of impedances that make up a given SWR. No special tools or graph paper are required. This can be done on the back of a napkin.

Let's suppose we have a coax line with Z_0 = 50 Ω, and we want to know the impedance range that would result in an SWR of 2. We can first calculate the resonant impedances — those with zero reactance — that would create an SWR of 2:

$$R_{\min} = Z_0 / \text{SWR} = 50 / 2 = 25\ \Omega$$
$$R_{\max} = Z_0 \times \text{SWR} = 50 \times 2 = 100\ \Omega$$

These are the only two pure resistances that will result in an SWR_{50} of 2, where SWR_{50} is the SWR in a 50 Ω system.

Now let's calculate the maximum reactance that would result in an SWR_{50} of 2,

$$X_{\max} = (R_{\max} - R_{\min})/2$$
$$= (100 - 25)/2 = 37.5\ \Omega$$

This is inductive reactance since the number is positive. The minimum possible capacitive reactance is simply the negative of this,

$$X_{\min} = X_{\max} \times (-1) = -37.5\ \Omega$$

For either of these values of reactance, the corresponding resistive part of the impedance is simply the average (midpoint) of the minimum and maximum resistance values:

$$R_{\text{avg}} = (R_{\max} + R_{\min})/2$$
$$= (100 + 25)/2 = 62.5\ \Omega$$

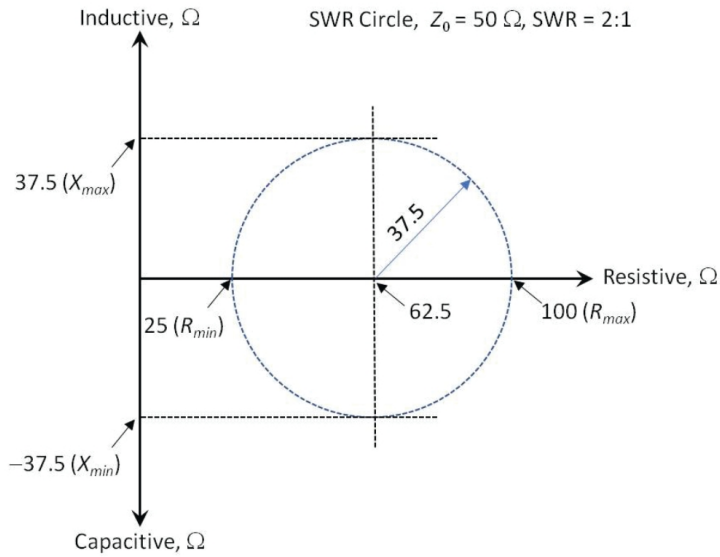

Figure 1 — SWR circle; Z_0 = 50 Ω and SWR = 2:1.

So the impedances at $X_{\max}$ and $X_{\min}$ are R = 62.5, X = 37.5 and R = 62.5 and X = –37.5 Ω or as complex numbers 62.5 + j37.5 and 62.5 – j37.5.

If you now graph this, see **Figure 1**, as a circle with a radius of 37.5 centered at the calculated midpoint of 62.5 on the x-axis, you would have a circle that represents all of the impedances that make up an SWR_{50} of 2. The x-axis is resistance and the y-axis is reactance.

Any combination of resistance and reactance that falls inside the circle will result in an SWR_{50} of less than 2, while any combination outside of the circle will result in an SWR_{50} greater than 2.

Those of you who enjoy working with Smith charts will notice the parallel technique but without the need for preprinted charts and normalization. Besides the SWR circle, there are many other SWR, reflection coefficient and impedance relations and derivations possible. — *73, Glenn Schulz, W9IQ, P.O. Box 1051, Branson, MO 65615;* **w9iq@arrl.net**.

Send your short *QEX* Technical Note to the Editor, via e-mail to qex@arrl.org. We reserve the right to edit your letter for clarity, and to fit in the available page space. "*QEX* Technical Note" may also appear in other ARRL media. The publishers of *QEX* assume no responsibilities for statements made by correspondents.

Upcoming Conferences

SCALE 20x

March 9-12, 2023

Pasadena, California

https://www.socallinuxexpo.org

The 20th Annual Southern California Linux Expo, SCALE 20x, will take place March 9 – 12, 2023, at the Pasadena Convention Center in Pasadena, California.

2023 SARA Western Conference

March 17-18, 2023

Bishop, California

www.radio-astronomy.org

The 2023 SARA Western Conference will be held at the Owens Valley Radio Observatory, Bishop, California, March 17-18, 2023.

New Mexico TechFest

March 18, 2023

Albuquerque, New Mexcio and Virtual

https://www.rmham.org/new-mexico-techfest/

A hybrid event this year, the New Mexico TechFest will be held at the UNM Continuing Education Conference Center in Albuquerque, New Mexico, and online via Zoom.

Microwave Update 2023 and 46th Eastern VHF/UHF Conference

April 14-15, 2023

Windsor, Connecticut

www.microwaveupdate.org

Microwave Update 2023 and the 46th Eastern VHF/UHF Conference will be held April 14 – 15, 2023, at the Hilton Garden Inn at Bradley Airport, Windsor, CT.

Aurora '23 Conference

June 3, 2023

Plymouth, MN

www.nlrs.club

Aurora ’23 will be held June 3, 2023, at the West Medicine Lake Community Club in Plymouth, Minnesota.

Eric P. Nichols, KL7AJ

AlasKit Educational and Scientific Resources, 3763 Lyle Ave., North Pole, AK 99705; **kl7aj72@gmail.com**

Self-Paced Essays – #16 Going Through a Phase

Phase is defined relative to a reference.

We mentioned in a previous essay that defining the phase angle of a non-repetitive signal is impossible. Let us revisit our simple *RC* circuit **Figure A** (Figure 1 from Essay #15), with which we demonstrated the *RC* time constant, as we explored last time, is also a low-pass filter.

We can certainly plot the voltage across C1 and the current through C1, **Figure 1**, and see the difference in timing between the two curves:

However, phase in its strict sense is undefined. *SPICE* modeling doesn't know what to do about phase when applied to a transient signal like this. So when speaking about phase, we need to confine our discussion to repetitive (harmonic) signals, of which the pure sine wave is the most straightforward to deal with.

Let us again drive this circuit with frequency swept ac signal (as in Essay #15), between 100 to 20,000 Hz and look at the amplitude response (**Figure 2**).

Now let us look at the phase angle. In *SPICE*, the phase angle is always the sampled node voltage relative to the voltage source. This may or may not tell us directly the phase displacement between voltage and current in a circuit, see **Figure 3**.

Without careful inspection we might conclude that the phase and amplitude response are the same. With more complex circuits we will see a profound difference.

In the next example, we take a look at a very simple series resonant circuit — the most rudimentary band-pass filter — and show this in **Figure 4**.

This circuit is resonant at 1.59 MHz, and has a very high Q. At the top of C1, the amplitude and phase response are shown in **Figure 5**.

The upper curve is the amplitude response, while the lower curve is the phase response. As you can see there is a sudden phase shift right at the resonant frequency. The higher the Q of the circuit, the more abrupt this phase shift will be.

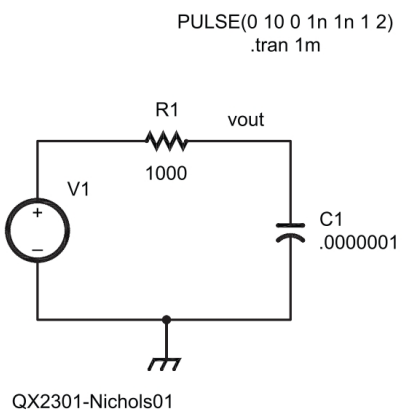

Figure A — A pulse driven *RC* circuit.

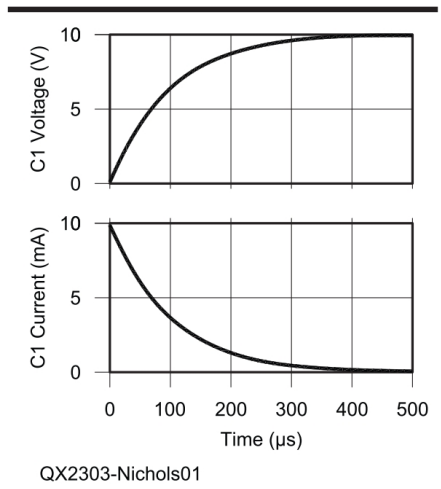

Figure 1 — Voltage at C1, and current through C1.

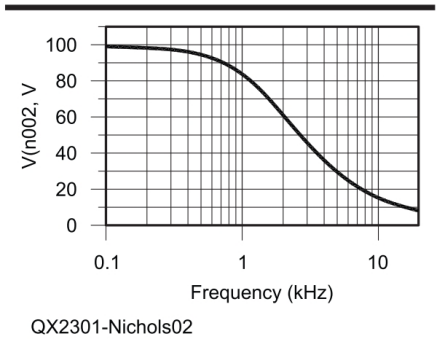

Figure 2 — Voltage at the junction of R1 and C1.

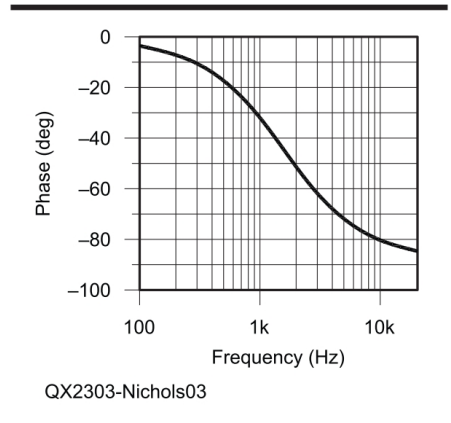

Figure 3 — Phase angle between the voltage at the junction of R1 and C1 and the current through C1.

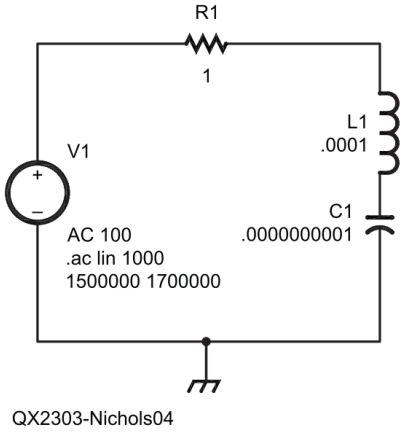

Figure 4 — A series resonant circuit.

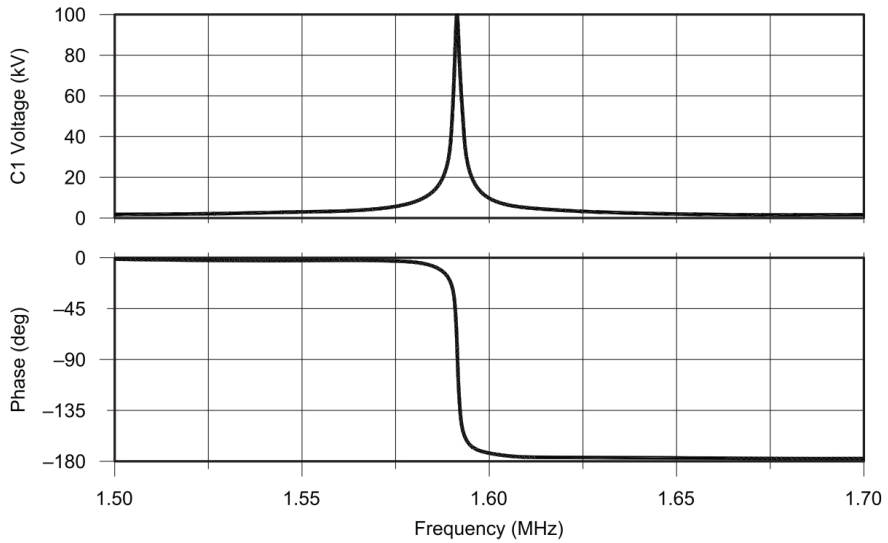

Figure 5 — The amplitude and phase at the top of C1.

Now, one might ask at this point, "just how important is the phase shift through a filter?" For any practical filter, don't we design it for a particular amplitude response? When do we care about the phase shift?

In many cases, phase shift is indeed not of particular importance. For a relatively narrow band IF strip in say, a communications receiver, we are not obsessively interested. We mentioned in Essay #15 how many of us radio technicians spent a lot of time performing IF alignment on numerous receivers. We didn't care about the phase shift, and even if we did, we didn't have any practical means of measuring it.

Where phase shift becomes of greater interest is in broadband signals. One prime example is in RADAR. Phase shift in an electrical circuit immediately implies time lag, and is closely related to propagation delay, which we will investigate in detail in a later essay. Referring to **Figure 3**, we see that the phase shift through a filter is frequency dependent.

In the case of a square wave — a very broadband signal indeed — we no longer have just one frequency, but a fundamental frequency and all the odd harmonics up to infinity. Fourier analysis shows this quite neatly. Now, if we're attempting to pass a square wave through a filter of some kind, we find that the lower frequency components pass through the circuit at a different rate than the higher frequency components. Since the different harmonics arrive at different times, we no longer have a square wave arriving at the output of the filter. So, we find that we definitely must be aware of the phase response of a filter in such a case.

As with every other aspect of engineering, we are always dealing with usable compromises. Not surprisingly, a filter designed for an optimum amplitude response will more often than not have a less than optimal phase response, and vice versa. This is why filter design has always been one of the most challenging aspects of radio engineering — and one of the reasons why digital signal processing (DSP) has become so popular and powerful — since optimizing both amplitude and phase response (nearly) simultaneously is greatly simplified.

Now, up to this point, we have considered only the "lumped constant" behavior of components. We have considered resistors, capacitors, and inductors to be contained at a specific point in space, with no consideration given to the time it takes for a current to flow through the particular component. We have, up to now, considered the "speed of electricity" to be infinite. The fact that phase shift can exist — and in this sense, again, we're talking about the difference in time between a voltage at one node of a circuit and the voltage at another node, not the displacement between voltage and current at a given node — hints that infinitely fast electricity is not the case. The existence of phase shift gives us a smooth transition into distributed components, such as transmission lines, which will be the subject of our next essay.

In preparation for the next essay, I will leave you with a homework assignment. Watch and fully absorb these videos: **https://youtu.be/DovunOxlY1k** and **https://youtu.be/I9m2w4DgeVk**. Until then, keep those soldering irons hot! — *73, Eric*.

Discover the Latest Ham Radio Gear at DX Engineering!

DX ENGINEERING New!

Iron Powder Cores

DX Engineering now carries popular material numbers and sizes of iron powder core toroids that can be used by amateur radio operators to build cost-effective RF inductors for MF to UHF circuit board applications, as well as for RF suppression. Their low permeability makes iron powder inductor cores preferred over ferrite in high-temperature environments inside hot equipment. Further, inductors wound on iron powder cores produce less electromagnetic interference to adjacent circuits. Choose from #2 (250 kHz-10 MHz) and #6 (3-40 MHz) toroids in packs of 5, 10, or 25. **Enter "Powder Core" at DXEngineering.com. From $19.99**

DX ENGINEERING

Aluminum Radio RF Ground Plane Kits

A less expensive alternative to DX Engineering's Copper Radio RF Ground Plane Kits, these aluminum versions are also effective in reducing stray RF pickup by indoor radio equipment and interconnecting cables. The kits include a pre-drilled 1/16-inch-thick aluminum sheet (13" x 10", 16" x 16", or 20" x 20") that is placed under your HF radios, microphones, and other devices, and connected to your existing grounding bus. The large surface area of metal improves upon the single-conductor grounding bus by equalizing the RF electric field around equipment and attached cables. This reduces voltage differences between pieces of equipment and the associated currents that cause RF interference to transceivers, microphones, tuners, amplifiers, computers, and other electronic equipment. Kits are available with or without an MDF mounting board. **Enter "DXE Aluminum Plane" at DXEngineering.com. From $49.99**

New!

Stick 500 Antenna Analyzer

RigExpert

New from the innovators at RigExpert comes the Stick 500, the latest addition to its lineup of easy-to-use, compact antenna analyzers that deliver in a big way. The Stick 500 (7.3" x 1.6" x 1.3") has a frequency range from 0.1.-500 MHz. It features a 3.7 V type 18650 Li-Ion battery; waterproof keyboard; high-contrast E Ink display; built-in Bluetooth; USB connection to a personal computer; SWR, return loss, R, X, Z, L, C, magnitude, and phase angle at one frequency modes; and mode for quick testing of a multi-band antenna. **Enter "Stick 500" at DXEngineering.com. REU-STICK-500 $399.95**

New!

Hi-Rate2 Headset with Foot Switch Packages

PARADAN radio New!

Here's a great combo sure to help you make more QSOs whether contesting or working DX. Hi-Rate2 packages offer an improved commercial-grade lightweight and comfortable stereo headset with sensitive electret boom microphone and wind shield to reduce breath popping noise; a ruggedly built and easy-to-activate "push-to-talk" foot switch that provides worry-free operating; cable assemblies; and transceiver mic adapter. With your hands free, you can enter call signs and reports on the keyboard, while switching from receive to transmit by depressing the foot switch. Six packages based on mic connector are available. **Enter "Hi-Rate2" at DXEngineering.com. From $115.00**

PicoAPRS and VHF Transceiver with GPS Receiver

WIMO

New!

Version 4 of the world's smallest APRS transceiver (1.30" x 2.60" x 1", 2.10 ounces) comes with a TNC and GPS receiver but now includes a VHF 2-meter handheld transceiver with PTT button, microphone, speaker, stored memories, color display, and more. Also new is the KISS data protocol for packet radio via a side-mounted USB-C socket, Bluetooth, or WiFi, making it easy to set up an APRS IGate. Transmit power is approximately 1 watt, switchable to 0.5 watts. Users will enjoy improved functionality from the new joystick-style front buttons. Depending on configuration, the device boasts a run time of up to 10 hours with its included 850 mAh Li-Ion battery. **Enter "PicoAPRS" at DXEngineering.com. WMO-PICOAPRS-VHF $399.99**

Coaxial RF Lightning and Surge Protectors

NexTek

New!

Safeguard your investment with NexTek. DX Engineering now carries several varieties of DC block and DC pass coaxial RF lightning surge protectors from NexTek—a company that has been designing, developing, and manufacturing solutions for hams and businesses worldwide since 1986. NexTek's PTC, PTI-BB50, and PTR series arrestors provide dependable, long-lasting wideband performance to protect equipment from electromagnetic pulse or power surges, while ensuring low SWR/insertion loss and no degradation of signal. **Enter "NexTek" at DXEngineering.com. From $55.00**

YAESU ICOM KENWOOD ALINCO HAMPLUS HEIL HAM RADIO OPTIBEAM butternut

Be a Better Ham! Check Out DX Engineering on Facebook and YouTube!

DX® ENGINEERING

Ordering (via phone) Country Code: +1
9 am to midnight ET, Monday-Friday
9 am to 5 pm ET, Weekends
Phone or e-mail Tech Support: 330-572-3200
9 am to 7 pm ET, Monday-Friday
9 am to 5 pm ET, Saturday
Email: DXEngineering@DXEngineering.com

Ohio Showroom Hours:
9 am to 5 pm ET, Monday-Saturday
Ohio Curbside Pickup:
9 am to 8 pm ET, Monday-Saturday
9 am to 7 pm ET, Sunday
Nevada Curbside Pickup:
9 am to 7 pm PT, Monday-Sunday

800-777-0703 | DXEngineering.com

ON ALL BANDS YouTube

Email Support 24/7/365 at DXEngineering@DXEngineering.com

Prices subject to change without notice. Please check DXEngineering.com for current pricing.

Cabin Fever? Spring into the new year with Icom

IC-V3500
2M Analog Transceiver

ID-52A
2M / 70CM
Analog / Digital Transceiver

NEW

IC-T10
2M / 70CM
Analog Transceiver

D-STAR ready

IC-705
Multi-band SDR
Portable Transceiver

IC-7300
HF / 6M SDR Transceiver

ID-5100A
2M / 70CM
Analog / Digital Transceiver

For the love of **ham radio.**

www.icomamerica.com/amateur
insidesales@icomamerica.com

ICOM®